

- Costinean, S., Sandhu, S.K., Pedersen, I.M., Tili, E., Trotta, R., Perrotti, D., Ciarlariello, D., Neviani, P., Harb, J., Kauffman, L.R., et al. (2009). Src homology 2 domain-containing inositol-5-phosphatase and CCAAT enhancer-binding protein beta are targeted by miR-155 in B cells of Emicro-MiR-155 transgenic mice. *Blood* 114, 1374–1382.
- Davis, B.N., and Hata, A. (2009). Regulation of MicroRNA Biogenesis: A miRiad of mechanisms. *Cell Commun. Signal.* 7, 18.
- Han, J., Pedersen, J.S., Kwon, S.C., Belair, C.D., Kim, Y.K., Yeom, K.H., Yang, W.Y., Haussler, D., Bilelloch, R., and Kim, V.N. (2009). Posttranscriptional crossregulation between Drosha and DGCR8. *Cell* 136, 75–84.
- Heo, I., Joo, C., Cho, J., Ha, M., Han, J., and Kim, V.N. (2008). Lin28 mediates the terminal uridylation of let-7 precursor MicroRNA. *Mol. Cell* 32, 276–284.
- Karube, Y., Tanaka, H., Osada, H., Tomida, S., Tatematsu, Y., Yanagisawa, K., Yatabe, Y., Takamizawa, J., Miyoshi, S., Mitsudomi, T., and Takahashi, T. (2005). Reduced expression of Dicer associated with poor prognosis in lung cancer patients. *Cancer Sci.* 96, 111–115.
- Kumar, M.S., Lu, J., Mercer, K.L., Golub, T.R., and Jacks, T. (2007). Impaired microRNA processing enhances cellular transformation and tumorigenesis. *Nat. Genet.* 39, 673–677.
- Larsen, J.E., Pavey, S.J., Passmore, L.H., Bowman, R., Clarke, B.E., Hayward, N.K., and Fong, K.M. (2007). Expression profiling defines a recurrence signature in lung squamous cell carcinoma. *Carcinogenesis* 28, 760–766.
- Li, T., Morgan, M.J., Choksi, S., Zhang, Y., Kim, Y.S., and Liu, Z.G. (2010). MicroRNAs modulate the noncanonical transcription factor NF-kappaB pathway by regulating expression of the kinase IKKalpha during macrophage differentiation. *Nat. Immunol.* 11, 799–805.
- Liang, J., Song, W., Tromp, G., Kolattukudy, P.E., and Fu, M. (2008a). Genome-wide survey and expression profiling of C/EBP-zinc finger family reveals a functional module in macrophage activation. *PLoS ONE* 3, e2880.
- Liang, J., Wang, J., Azfer, A., Song, W., Tromp, G., Kolattukudy, P.E., and Fu, M. (2008b). A novel C/EBP-zinc finger protein family regulates proinflammatory activation of macrophages. *J. Biol. Chem.* 283, 6337–6346.
- Lu, J., Getz, G., Miska, E.A., Alvarez-Saavedra, E., Lamb, J., Peck, D., Sweet-Cordero, A., Ebert, B.L., Mak, R.H., Ferrando, A.A., et al. (2005). MicroRNA expression profiles classify human cancers. *Nature* 435, 834–838.
- Martello, G., Rosato, A., Ferrari, F., Manfrin, A., Cordenonsi, M., Dupont, S., Enzo, E., Guzzardo, V., Rondina, M., Spruce, T., et al. (2010). A MicroRNA targeting dicer for metastasis control. *Cell* 141, 1195–1207.
- Matsushita, K., Takeuchi, O., Standley, D.M., Kumagai, Y., Kawagoe, T., Miyake, T., Satoh, T., Kato, H., Tsujimura, T., Nakamura, H., and Akira, S. (2009). Zc3h12a is an RNase essential for controlling immune responses by regulating mRNA decay. *Nature* 458, 1185–1190.
- Melo, S.A., Moutinho, C., Roperio, S., Calin, G.A., Rossi, S., Spizzo, R., Fernandez, A.F., Davalos, V., Villanueva, A., Montoya, G., et al. (2010). A genetic defect in exportin-5 traps precursor microRNAs in the nucleus of cancer cells. *Cancer Cell* 18, 303–315.
- Merritt, W.M., Lin, Y.G., Han, L.Y., Kamat, A.A., Spannuth, W.A., Schmandt, R., Urbauer, D., Pennacchio, L.A., Cheng, J.F., Nick, A.M., et al. (2008). Dicer, Drosha, and outcomes in patients with ovarian cancer. *N. Engl. J. Med.* 359, 2641–2650.
- Moschos, S.A., Williams, A.E., Perry, M.M., Birrell, M.A., Belvisi, M.G., and Lindsay, M.A. (2007). Expression profiling in vivo demonstrates rapid changes in lung microRNA levels following lipopolysaccharide-induced inflammation but not in the anti-inflammatory action of glucocorticoids. *BMC Genomics* 8, 240.
- Nagel, R., le Sage, C., Diosdado, B., van der Waal, M., Oude Vrielink, J.A., Bolijn, A., Meijer, G.A., and Agami, R. (2008). Regulation of the adenomatous polyposis coli gene by the miR-135 family in colorectal cancer. *Cancer Res.* 68, 5795–5802.
- O'Connell, R.M., Rao, D.S., Chaudhuri, A.A., and Baltimore, D. (2010). Physiological and pathological roles for microRNAs in the immune system. *Nat. Rev. Immunol.* 10, 111–122.
- Ozen, M., Creighton, C.J., Ozdemir, M., and Ittmann, M. (2008). Widespread deregulation of microRNA expression in human prostate cancer. *Oncogene* 27, 1788–1793.
- Paschoud, S., Dogar, A.M., Kuntz, C., Grisoni-Neupert, B., Richman, L., and Kühn, L.C. (2006). Destabilization of interleukin-6 mRNA requires a putative RNA stem-loop structure, an AU-rich element, and the RNA-binding protein AUF1. *Mol. Cell. Biol.* 26, 8228–8241.
- Ramachandran, V., and Chen, X. (2008). Degradation of microRNAs by a family of exoribonucleases in Arabidopsis. *Science* 321, 1490–1492.
- Rodriguez, A., Vigorito, E., Clare, S., Warren, M.V., Couttet, P., Soond, D.R., van Dongen, S., Grocock, R.J., Das, P.P., Miska, E.A., et al. (2007). Requirement of bic/microRNA-155 for normal immune function. *Science* 316, 608–611.
- Ruggiero, T., Trabucchi, M., De Santa, F., Zupo, S., Harfe, B.D., McManus, M.T., Rosenfeld, M.G., Briata, P., and Gherzi, R. (2009). LPS induces KH-type splicing regulatory protein-dependent processing of microRNA-155 precursors in macrophages. *FASEB J.* 23, 2898–2908.
- Sadler, A.J., and Williams, B.R. (2008). Interferon-inducible antiviral effectors. *Nat. Rev. Immunol.* 8, 559–568.
- Salehzada, T., Silhol, M., Steff, A.M., Lebleu, B., and Bisbal, C. (1993). 2',5'-Oligoadenylate-dependent RNase L is a dimer of regulatory and catalytic subunits. *J. Biol. Chem.* 268, 7733–7740.
- Sandberg, R., Neilson, J.R., Sarma, A., Sharp, P.A., and Burge, C.B. (2008). Proliferating cells express mRNAs with shortened 3' untranslated regions and fewer microRNA target sites. *Science* 320, 1643–1647.
- Shedden, K., Taylor, J.M., Enkemann, S.A., Tsao, M.S., Yeatman, T.J., Gerald, W.L., Eschrich, S., Jurisica, I., Giordano, T.J., Misek, D.E., et al; Director's Challenge Consortium for the Molecular Classification of Lung Adenocarcinoma. (2008). Gene expression-based survival prediction in lung adenocarcinoma: a multi-site, blinded validation study. *Nat. Med.* 14, 822–827.
- Siomi, H., and Siomi, M.C. (2010). Posttranscriptional regulation of microRNA biogenesis in animals. *Mol. Cell* 38, 323–332.
- Subramanian, A., Tamayo, P., Mootha, V.K., Mukherjee, S., Ebert, B.L., Gillette, M.A., Paulovich, A., Pomeroy, S.L., Golub, T.R., Lander, E.S., and Mesirov, J.P. (2005). Gene set enrichment analysis: a knowledge-based approach for interpreting genome-wide expression profiles. *Proc. Natl. Acad. Sci. USA* 102, 15545–15550.
- Suzuki, H.I., and Miyazono, K. (2010). Dynamics of microRNA biogenesis: crosstalk between p53 network and microRNA processing pathway. *J. Mol. Med.* 88, 1085–1094.
- Suzuki, H.I., and Miyazono, K. (2011). Emerging complexity of microRNA generation cascades. *J. Biochem.* 149, 15–25.
- Suzuki, H.I., Yamagata, K., Sugimoto, K., Iwamoto, T., Kato, S., and Miyazono, K. (2009). Modulation of microRNA processing by p53. *Nature* 460, 529–533.
- Umbach, J.L., and Cullen, B.R. (2009). The role of RNAi and microRNAs in animal virus replication and antiviral immunity. *Genes Dev.* 23, 1151–1164.
- Wu, H., Neilson, J.R., Kumar, P., Manocha, M., Shankar, P., Sharp, P.A., and Manjunath, N. (2007). miRNA profiling of naïve, effector and memory CD8 T cells. *PLoS ONE* 2, e1020.
- Xiao, C., Srinivasan, L., Calado, D.P., Patterson, H.C., Zhang, B., Wang, J., Henderson, J.M., Kutok, J.L., and Rajewsky, K. (2008). Lymphoproliferative disease and autoimmunity in mice with increased miR-17-92 expression in lymphocytes. *Nat. Immunol.* 9, 405–414.
- Zhang, H., Kolb, F.A., Jaskiewicz, L., Westhof, E., and Filipowicz, W. (2004). Single processing center models for human Dicer and bacterial RNase III. *Cell* 118, 57–68.
- Zuker, M. (2003). Mfold web server for nucleic acid folding and hybridization prediction. *Nucleic Acids Res.* 31, 3406–3415.

Overexpression of enhancer of zeste homolog 2 with trimethylation of lysine 27 on histone H3 in adult T-cell leukemia/lymphoma as a target for epigenetic therapy

Daisuke Sasaki,¹ Yoshitaka Imaizumi,² Hiroo Hasegawa,¹ Akemi Osaka,¹ Kunihiro Tsukasaki,² Young Lim Choi,³ Hiroyuki Mano,³ Victor E. Marquez,⁴ Tomayoshi Hayashi,⁵ Katsunori Yanagihara,¹ Yuji Moriwaki,² Yasushi Miyazaki,² Shimeru Kamihira,¹ and Yasuaki Yamada¹

¹Department of Laboratory Medicine, Nagasaki University Graduate School of Biomedical Sciences, Nagasaki, Japan; ²Department of Hematology and Molecular Medicine, Atomic Bomb Disease Institute, Nagasaki University Graduate School of Biomedical Sciences, Nagasaki, Japan; ³Division of Functional Genomics, Jichi Medical University, Tochigi, Japan; ⁴Chemical Biology Laboratory, National Cancer Institute, Frederick, MD, USA; and ⁵Department of Pathology, Nagasaki University Hospital, Nagasaki, Japan

ABSTRACT

Background

Enhancer of zeste homolog 2 is a component of the Polycomb repressive complex 2 that mediates chromatin-based gene silencing through trimethylation of lysine 27 on histone H3. This complex plays vital roles in the regulation of development-specific gene expression.

Design and Methods

In this study, a comparative microarray analysis of gene expression in primary adult T-cell leukemia/lymphoma samples was performed, and the results were evaluated for their oncogenic and clinical significance.

Results

Significantly higher levels of Enhancer of zeste homolog 2 and RING1 and YY1 binding protein transcripts with enhanced levels of trimethylation of lysine 27 on histone H3 were found in adult T-cell leukemia/lymphoma cells compared with those in normal CD4⁺ T cells. Furthermore, there was an inverse correlation between the expression level of Enhancer of zeste homolog 2 and that of miR-101 or miR-128a, suggesting that the altered expression of the latter miRNAs accounts for the overexpression of the former. Patients with high Enhancer of zeste homolog 2 or RING1 and YY1 binding protein transcripts had a significantly worse prognosis than those without it, indicating a possible role of these genes in the oncogenesis and progression of this disease. Indeed, adult T-cell leukemia/lymphoma cells were sensitive to a histone methylation inhibitor, 3-deazaneplanocin A. Furthermore, 3-deazaneplanocin A and histone deacetylase inhibitor panobinostat showed a synergistic effect in killing the cells.

Conclusions

These findings reveal that adult T-cell leukemia/lymphoma cells have deregulated Polycomb repressive complex 2 with over-expressed Enhancer of zeste homolog 2, and that there is the possibility of a new therapeutic strategy targeting histone methylation in this disease.

Key words: adult T-cell leukemia/lymphoma, human T-cell leukemia virus type-1, Enhancer of zeste homolog 2, H3K27me3.

Citation: Sasaki D, Imaizumi Y, Hasegawa H, Osaka A, Tsukasaki K, Choi YL, Mano H, Marquez VE, Hayashi T, Yanagihara K, Moriwaki Y, Miyazaki Y, Kamihira S, and Yamada Y. Overexpression of enhancer of zeste homolog 2 with trimethylation of lysine 27 on histone H3 in adult T-cell leukemia/lymphoma as a target for epigenetic therapy *Haematologica* 2011;96(4):712-719. doi:10.3324/haematol.2010.028605

©2011 Ferrata Storti Foundation. This is an open-access paper.

Funding: supported in part by a Grant-in-Aid for Scientific Research from the Ministry of Health, Labour, and Welfare of Japan (N. 04010119). For VEM, this research was supported in part by the Intramural Research Program of the NIH, Center for Cancer Research, NCI-Frederick.

Acknowledgments: the authors thank Sayaka Mori and Yuko Doi for excellent technical assistance.

Manuscript received June 16, 2010. *Revised version arrived* on December 16, 2010. *Manuscript accepted on* December 31, 2010.

Correspondence: Yasuaki Yamada, Department of Laboratory Medicine, 1-7-1 Sakamoto, Nagasaki 852-8501, Japan. Phone: international +81.958197408. Fax: international +81.958197422. E-mail: y-yamada@nagasaki-u.ac.jp

The online version of this article has a Supplementary Appendix.

Introduction

The Polycomb group (PcG) proteins play critical roles in the regulation of development by repressing specific sets of developmental genes through chromatin modification.¹ They form two distinct multimeric complexes, Polycomb repressive complex 1 (PRC1) and PRC2, which bind to polycomb responsive elements (PRE), repress genes required for cell differentiation, and maintain pluripotency and self-renewal of embryonic stem cells and hematopoietic stem cells.^{2,3} PRC2 consists of Enhancer of zeste homolog 2 (EZH2), which has histone methyltransferase activity, suppressor of zeste 12 (SUZ12), and embryonic ectoderm development (EED), which is required to maintain the integrity of PRC2.^{1,4} Sequence-specific DNA binding protein YY1, which recognizes PRE, interacts with EED and recruits PRC2 to a specific chromatin domain to be repressed.⁵ EED interacts with histone deacetylase (HDAC) proteins, HDAC1 and HDAC2, and the histone binding proteins RBBP4 (RbAp48) and RBBP7 (RbAp46).⁶ PRC2 thus also participates in histone deacetylation. EZH2, as a part of the PRC2 complex, not only methylates histone but also serves as a recruitment platform for DNA methyltransferases that methylate the promoter regions of target genes, which is another mechanism of gene repression.⁷ The more diverse complex PRC1 consists of HPC family proteins that mediate chromatin association, HPH family proteins, RING, BMI1, and others.¹ PRC2 initiates trimethylation of lysine 27 on histone H3 (H3K27me3) and, to a lesser extent, lysine 9 of histone H3.⁸ PRC1 recognizes H3K27me3 through the chromodomain of the HPC and maintains the trimethylation. There are a number of reports indicating that such epigenetically mediated transcriptional silencing is associated with cancer development.^{1,9} Among these, oncogenic roles of over-expressed EZH2 have been studied in a variety of tumors.¹⁰

Adult T-cell leukemia/lymphoma (ATL) is a neoplasm of mature CD4⁺ T-cell origin, etiologically associated with human T-cell leukemia virus type-1 (HTLV-1).^{11,12} Its clinical behavior differs among patients and is subclassified into four subtypes: smoldering type and chronic type as indolent subtypes, and acute type and lymphoma type as aggressive subtypes.¹³ Inactivation of tumor suppressor genes is one of the key events in development and progression, and there is a strong accumulation of *p14ARF/p15INK4B/p16INK4A* gene deletion/methylation or *p53* gene mutations in aggressive subtypes (>60%).^{14,20} In the present study, for further investigation of the oncogenesis of ATL, we performed a comparative microarray analysis of gene expression in primary ATL samples. ATL cells expressed significantly higher levels of *EZH2* and *RYBP* (RING1 and YY1 binding protein) transcripts than CD4⁺ T cells from healthy volunteers. Moreover, acute-type ATL cells showed significantly higher levels of these transcripts than chronic-type ATL cells, suggesting that deregulation of PcG proteins plays a crucial role not only in the development but also in the progression of ATL. In addition, ATL samples were strongly positive for H3K27me3, and were sensitive to 3-deazaneplanocin A (DZNep), a histone methylation inhibitor.^{21,23} It has recently been shown that HDAC inhibitor panobinostat (PS, also known as LBH589) depletes the levels of EZH2, SUZ12, and EED and induces apoptotic death in leukemia cells.²⁴ Deregulation of PcG protein genes with over-

expressed EZH2 in ATL cells suggests that ATL is one of the appropriate target diseases for such epigenetic therapy.

Design and Methods

Sample preparation

This study was approved by the ethics committees of Nagasaki University, and all clinical samples were obtained after written informed consent was provided. The diagnosis of ATL was confirmed by the monoclonal integration of HTLV-1 proviral DNA in the genomic DNA of leukemia cells. Peripheral blood mononuclear cells (PBMCs) were obtained from ATL patients (acute type 22 cases, chronic type 19 cases) and healthy adult volunteers by density gradient centrifugation using Lympho-prep (AXIS SHIELD, Oslo, Norway). For enrichment of ATL cells, CD4⁺ cells were purified from the PBMCs by the magnetic bead method (CD4 MicroBeads, Miltenyi Biotec, Auburn, CA, USA) as described elsewhere.²⁵ Besides these samples for microarray analysis, we prepared another set of samples for quantitative real-time RT-PCR (qRT-PCR) and Western blotting (25 ATL patients, 13 HTLV-1 carriers, and 12 healthy adults) to confirm the results of microarray analysis. We also used formalin-fixed, paraffin-embedded lymph nodes from 7 patients with lymphoma-type ATL and 5 patients with follicular lymphoma for immunohistochemical analysis.

ATL cell lines used in this study, SO4, ST1, KK1, KOB, and LM-Y1, were established from respective patients in our laboratory and have been confirmed to be of primary ATL cell origin.²⁶ Cells were maintained in RPMI1640 medium supplemented with 10% FBS and 100 Japan reference units of recombinant interleukin-2 (rIL-2) (kindly provided by Takeda Pharmaceutical Company, Ltd., Osaka, Japan). We also used HTLV-1-infected T-cell lines MT2 and HuT102 and acute T-lymphoblastic leukemia cell lines Jurkat and MOLT4, which were maintained without rIL-2.

DNA microarray analysis

RNA was prepared from purified CD4⁺ T cells, and subjected to hybridization to HGU133A & B microarray containing 44,760 probe sets for human genes (Affymetrix, Santa Clara, CA, USA) as described previously.^{25,27} The mean expression intensity of the internal positive control probe sets (http://www.affymetrix.com/support/technical/mask_files.affx) was set to 500 units in each hybridization, and the fluorescence intensity of each test gene was normalized accordingly. All HGU133A & B microarray data are available from the Gene Expression Omnibus website (<http://www.ncbi.nlm.nih.gov/geo>) under the accession number GSE1466.

Quantitative real-time RT-PCR

For confirmation of the results of microarray analysis, we performed quantitative real-time RT-PCR (qRT-PCR) for PcG protein genes. Total RNA was prepared using Isogen (Wako, Osaka, Japan). After removal of contaminated DNA with DNase (Message Clean kit; GenHunter, Nashville, TN, USA), cDNA was constructed from 1 µg of total RNA using the SuperScript III RT-PCR System (Invitrogen, Carlsbad, CA, USA) according to the manufacturer's instructions. Primers and TaqMan probes labeled with TAMRA dye at the 3' end and FAM at the 5' end are listed in Online Supplementary Table S1. The mRNA levels for PcG family proteins and porphobilinogen deaminase (PBGD) were measured from a cDNA template using a LightCycler480 PCR System (Roche Diagnostics, Mannheim, Germany). Briefly, reactions were performed in a 20 µL volume with 5 µL (25 ng) of cDNA, 0.5 µM PCR primers, 0.1 µM TaqMan probes, and 10 µL of LightCycler

480 probes Master Mix (Roche Diagnostics). The PCR program consisted of 95°C for 5 min followed by 50 cycles of 95°C for 10 sec and 60°C for 30 sec. After 50 cycles, the absolute amounts of PcG protein mRNA and *PBGD* mRNA were interpolated from the standard curves generated by the dilution method using plasmids derived from a clone transfected with pTAC-1 Vector (BioDynamics Laboratory Inc., Tokyo, Japan) containing amplicons from the PcG family protein and *PBGD* genes, respectively. To normalize these results for variability in concentration and integrity of RNA and cDNA, the *PBGD* gene was used as an internal control in each sample.

For the quantitative PCR for microRNAs (miRNAs), miR-101, miR-26a, and miR-128a, 10 ng of total RNA (containing miRNA) was used. RT reaction and real-time quantification were performed using TaqMan MicroRNA RT kit and TaqMan MicroRNA assays (hsa-miR-26a, assay ID 000405; hsa-miR-101, assay ID 002253; hsa-miR-128a, assay ID 002216; RNU6B, assay ID 001093) (Applied Biosystems, Foster City, CA, USA) in accordance with the manufacturer's instructions. Each PCR reaction mixture contained 10 µL of LightCycler 480 probes Master Mix, 4 µL of nuclease-free water, 1 µL of 20X specific PCR primer, and 5 µL of RT product. The thermal cycle was programmed as follows: 95°C for 5 min, 40 cycles of 95°C for 15 sec, and 60°C for 60 sec. Using the comparative CT method, we used an endogenous control (RNU6B) to normalize the expression levels of target micro-RNA by correcting differences in the amount of RNA loaded into qPCR reactions.

Western blot analysis and antibodies

Western blot analysis was performed as described previously.²⁸ The analysis was performed using antibodies to EZH2 and Histone H3 (Cell Signaling Technology, Danvers, MA, USA), phospho EZH2 (Ser21) (Bethyl Laboratories, Montgomery, TX, USA), H3K27me3, dimethylated H3K27 (H3K27me2), monomethylated H3K27 (H3K27me1) (Millipore, Temecula, CA, USA), and β -actin (Sigma, St. Louis, MO, USA).

Immunohistochemistry

Immunohistochemical staining for EZH2 and H3K27me3 was performed on formalin-fixed, paraffin-embedded lymph node samples from lymphoma-type ATL patients and follicular lymphoma patients as a control. The deparaffinized slides were pretreated with DAKO Target Retrieval Solution, pH 9 (DAKO Japan, Tokyo, Japan), and heated in a water bath at 95°C for 40 min. For all stains, the endogenous peroxidase was quenched using 3% H₂O₂ for 15 min. Sections were then placed in 0.5% non-fat dry milk for 30 min at room temperature. The primary antibodies used were anti-EZH2 antibody (BD Biosciences, San Jose, CA, USA) and anti-H3K27me3 antibody (Cell Signaling Technology, Boston, MA, USA), and were applied at 1:50 dilution and 1:100 dilution, respectively. They were allowed to react for 1 h at room temperature, and then the DAKO EnVision™ + Dual Link System-HRP (DAKO Japan, Tokyo, Japan) was applied using diaminobenzidine as the chromogen, following the manufacturer's protocol.

Sensitivity of adult T-cell leukemia/lymphoma cell lines to DZNep and PS (LBH589)

DZNep was synthesized by one of the authors (VEM). Cells were treated with different concentrations of DZNep for 72 h and the cell proliferation status was evaluated by an MTS assay using a Cell Titer 96® AQueous Cell Proliferation Assay kit (Promega, Madison, WI, USA) in accordance with the manufacturer's instructions. To analyze the synergistic effect of combined treatment with DZNep and PS (LBH589) (kindly provided by Novartis Pharma AG, Basel, Switzerland), cells were treated with DZNep

(0.3–5.0 µM) and PS (LBH589) (3–50 nM) for 48 h. After the cell proliferation status was evaluated by an MTS assay, the combination index (CI) for each drug combination was obtained by determining the median dose effect of Chou and Talalay using the CI equation within the commercially available software Calcsyn (Biosoft).²⁹ CI < 1, CI = 1, and CI > 1 indicate synergism, additive effect, and antagonism, respectively. Cell viability represents the value relative to that of the control culture without these agents.

Results

Microarray analysis shows increased EZH2 and/or RYBP transcripts in adult T-cell leukemia/lymphoma cells

In a comparative microarray analysis of primary ATL samples, we focused on investigating PcG protein genes, *EZH2*, *RYBP*, *BMI-1*, and *CBX7*, in the present study because ATL cells show many aberrantly hypermethylated DNA sequences.³⁰ ATL cells expressed significantly higher levels of *EZH2* and *RYBP* transcripts than CD4⁺ T cells from healthy adults (Figure 1A and B). In addition, there was a difference between ATL subtypes in these expressions, and cells from the acute type showed significantly higher levels of these transcripts than the cells from the chronic type. When patients were separated into two groups consisting of those with high expression and those with low expression, the group with high *EZH2* or high *RYBP* transcript showed significantly shorter survival than the respective low-expression groups (Figure 1E and F), indicating that high *EZH2* and/or *RYBP* expression is associated with aggressive clinical behavior. Convincingly, there was a trend toward accumulation of acute-type ATL in the high *EZH2* or the high *RYBP* expression group: 14 cases of acute type and 6 cases of chronic type in the high *EZH2* group, 7 cases of acute type and 13 cases of chronic type in the low *EZH2* group, 14 cases of acute type and 6 cases of chronic type in the high *RYBP* group, and 7 cases of acute type and 13 cases of chronic type in the low *RYBP* group. BMI1 is known to down-regulate the expression of *p14ARF/p16INK4A* and lead to neoplastic transformation.³¹ Chromobox 7 (*CBX7*), a component of the PRC1, is also known to repress the transcription of *p14ARF/p16INK4A*.³² Since inactivation of *p14ARF/p15INK4B/p16INK4A* genes is one of the key events in ATL progression, expression of *BMI-1* and/or *CBX7* transcript was expected to be elevated in acute-type ATL cells. There was, however, no difference in these expressions between ATL subtypes or even between ATL cells and normal CD4⁺ T cells (Figure 1C and D). There was no difference in survival for different *BMI-1* or *CBX7* expression levels (Figure 1G and H).

Confirmation of increased EZH2 and/or RYBP transcripts by quantitative real-time RT-PCR

For confirmation of the results of microarray analysis, we quantified the transcripts of the PcG protein genes including *EZH2* and *RYBP* by qRT-PCR using another set of samples from ATL patients, healthy adults, HTLV-1 carriers, and hematologic cell lines including ATL cell lines. In accordance with the results of microarray analysis, *EZH2* and *RYBP* transcripts were increased in primary ATL cells compared with those in the cells from healthy adults and HTLV-1 carriers, with statistically significantly higher val-

ues in *EZH2* in terms of both absolute copy number per 25 ng of total RNA and normalized expression level (Online Supplementary Figure S1A, a, B, b). *RBBP4* was significantly higher in primary ATL cells than in the cells from healthy adults and HTLV-1 carriers in terms of normalized expression level (Online Supplementary Figure S1 C, c). In contrast, there was no difference in *BMI1*, *YY1*, and *EED* expressions among these groups, although some patients showed very high *BMI1* expression (Online Supplementary Figure S1D, d, E, e, F, f). Similarly to primary ATL cells, some ATL cell lines showed high *EZH2* expression in terms of absolute copy number per 25 ng of total RNA (Online Supplementary Figure S1A).

***EZH2* protein expression with trimethylation of H3K27 is characteristic in adult T-cell leukemia/lymphoma cells**

We then examined *EZH2* and *RYBP* at the protein level by Western blotting. A 98-kDa band for *EZH2* protein and a 32-kDa band for *RYBP* protein were detected in all primary ATL samples irrespective of subtype, but they were hardly detected in cells from healthy adults and HTLV-1

carriers (Figure 2A, Online Supplementary Figure S2, and data not shown). ATL cell lines and acute T-lymphoblastic leukemia cell lines also showed intense *EZH2* bands. The serine-threonine kinase Akt phosphorylates *EZH2* at serine 21 and suppresses its methyltransferase activity by impeding *EZH2* binding to histone H3, which results in a decrease in lysine 27 trimethylation.³³ *EZH2* of ATL cells was not phosphorylated and was in its active form (Figure 2A). In fact, most primary ATL samples showed the band for H3K27me3, while the cells from healthy adults lacked the band (Figure 2B). As it is known that *EZH2* plays a crucial role in trimethylation but not in dimethylation or monomethylation, the bands for H3K27me2 and H3K27me1 were detected in all samples examined, but the band for H3K27me3 was limited in primary ATL cells and ATL cell lines LMY1 and KOB that showed an intense *EZH2* band with a faint phosphorylated *EZH2* band (Figure 2A and B). In contrast, *EZH2* was strongly phosphorylated in ATL cell lines ST1, SO4, KK1, and acute T-lymphoblastic leukemia cell lines Jurkat and MOLT4, and these cell lines hardly showed the band for H3K27me3. Collectively, these results indicate that ATL cells express

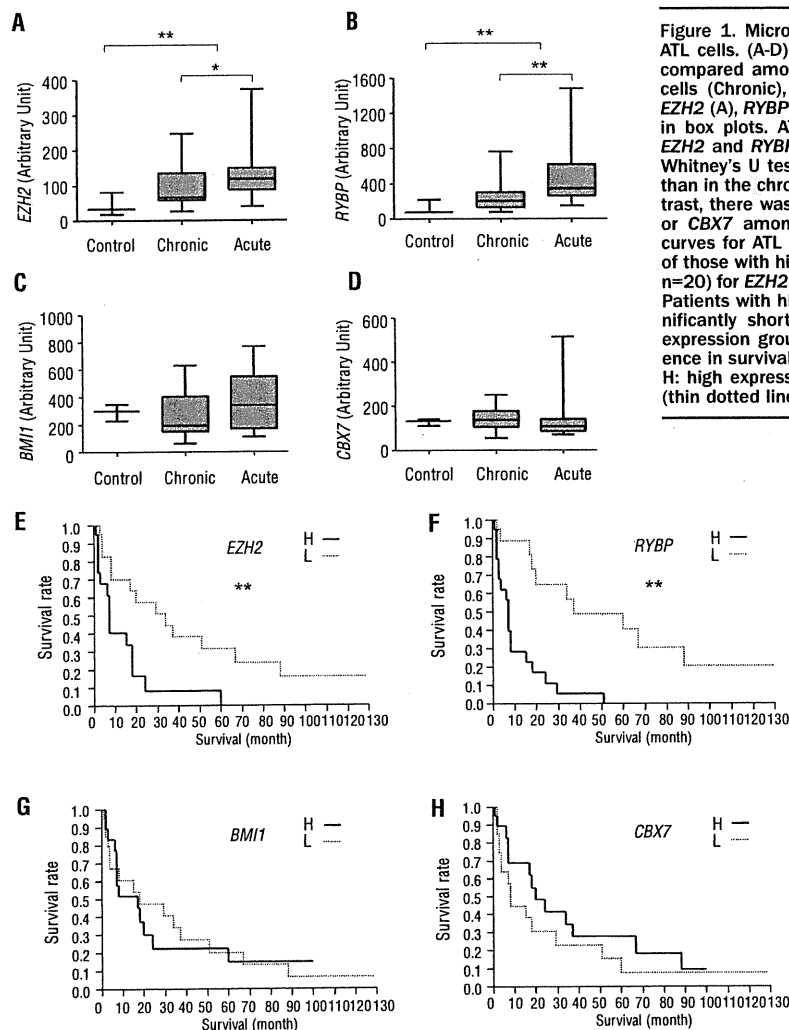


Figure 1. Microarray analysis of gene expression in primary ATL cells. (A-D) Expression levels of PcG protein genes were compared among normal CD4⁺ T cells (Control), chronic ATL cells (Chronic), and acute ATL cells (Acute), and results of *EZH2* (A), *RYBP* (B), *BMI1* (C), and *CBX7* (D) are demonstrated in box plots. ATL cells showed significantly higher levels of *EZH2* and *RYBP* transcripts than normal CD4⁺ T cells (Mann-Whitney's U test), with a higher expression in the acute type than in the chronic type (Mann-Whitney's U test) (A, B). In contrast, there was no statistical difference in the level for *BMI1* or *CBX7* among these groups (C, D). (E-H) Overall survival curves for ATL patients separated into two groups consisting of those with high expression (H, n=20) and low expression (L, n=20) for *EZH2* (E), *RYBP* (F), *BMI1* (G), or *CBX7* (H) are shown. Patients with high *EZH2* or high *RYBP* expression showed significantly shorter survival than those in corresponding low expression groups (log rank test) (E, F). There was no difference in survival for different *BMI1* or *CBX7* expressions (G, H). H: high expression group (bold line), L: low expression group (thin dotted line). **P*<0.05, ***P*<0.01

functionally active EZH2, and as a result, their H3K27 are trimethylated, and that ATL cell lines LMY1 and KOB preserve this characteristic of primary ATL cells.

Immunohistochemical confirmation of the expression of EZH2 and H3K27me3 in lymph nodes

We next used lymph nodes from lymphoma-type ATL patients for immunohistochemical evaluation of EZH2 expression and H3K27me3. In agreement with the results of Western blotting, all ATL lymph nodes from 7 patients were strongly positive for both EZH2 and H3K27me3 without exception in their nuclear staining (*Online Supplementary Figure S3 and data not shown*), suggesting that overexpression of EZH2 with H3K27me3 is a common feature of ATL cells irrespective of ATL subtypes. In

contrast, in lymph nodes from 5 follicular lymphoma patients, only a few cells were positive for EZH2 with some variation among patients and most cells were negative for H3K27me3 (*Online Supplementary Figure S3 and data not shown*).

Downregulation of miR-101 and miR-128a may be responsible for increased EZH2 expression

So far, more than 700 miRNAs have been identified in humans, and each miRNA regulates multiple target genes. miR-101 and miR-26a have been shown to be negative regulators of *EZH2* expression and are depressed in several types of cancer cells.^{34,35} miR-128a is known to be a negative regulator of *BMI1* and has been reported to be involved in glioma cell proliferation.³⁶ We quantified these miRNAs in primary ATL cells and cells from HTLV-1 carriers to investigate the mechanism of *EZH2* overexpression. ATL cells showed significantly decreased levels of miR-101 and miR-128a compared with the cells from HTLV-1 carriers (*Figure 3A and C*). Notably, there were significant inverse correlations between *EZH2* expression and miR-101 expression or *EZH2* expression and miR-128a expression (*Figure 3D and E*), suggesting that decrease of these miRNAs accounts for the overexpression of *EZH2*. Since genomic loss of miR-101 has been reported in prostate cancer,³⁴ we performed quantitative genomic PCR for miR-101 in two loci, miR-101-1 (chromosome 1p31) and miR-101-2 (chromosome 9p24). Both loci were preserved in all 10 ATL samples examined (*Online Supplementary Figure S4*). The expression of miR-26a did not, in contrast, differ between ATL cells and cells from HTLV-1 carriers (*Figure 3B*). Unexpectedly, there was no significant correlation between *BMI1* expression and miR-128a expression (*Figure 3F*).

Adult T-cell leukemia/lymphoma cells are sensitive to DZNep and PS (LBH589)

We first examined the sensitivity of ATL-related cell lines and acute T-lymphoblastic leukemia cell lines to DZNep, an inhibitor of S-adenosylhomocysteine hydrolyase, which has recently been shown to decrease the expression of EZH2 and histone methylation.^{22,23} DZNep inhibited the proliferation of these cell lines, at concentrations above 0.5 μ M (*Online Supplementary Figure S5A*). In contrast, CD4⁺ T cells from healthy adults as a normal control were resistant to DZNep even at 5 μ M. Notably, although DZNep decreased *EZH2* expression in ST1, SO4, and KK1, it did not decrease but rather increased the expression in KOB, results which were confirmed by Western blot (*Online Supplementary Figure S5B and C*). PS (LBH589) is also known to decrease the level of EZH2 in several types of leukemia cells.²⁴ One hundred nM of PS (LBH589) decreased *EZH2* expression at both transcript and protein levels in ATL cell lines including KOB and LM-Y1, which showed a similar *EZH2* expression profile to that of primary ATL cells, namely, high *EZH2* expression with low phosphorylated EZH2 and strong H3K27me3 (*Online Supplementary Figure S5D and E*). We next examined whether these agents show a synergistic effect or just an additive effect. As shown in *Online Supplementary Figure S5F* (upper panel), the cell viabilities of LM-Y1 treated with 25 nM PS (LBH589) or 2.5 μ M DZNep were 70% and 87%, respectively. A combination of this setting (LBH:DZNep=1:100) markedly decreased the proportion of viable cells (40%) compared with that of cells treated

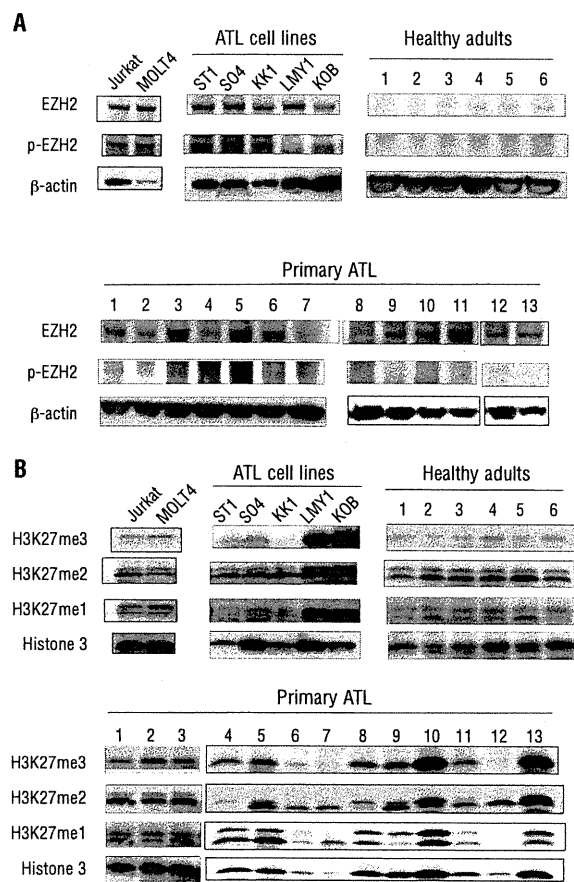


Figure 2. EZH2 protein expression and histone methylation. (A) Western blot analysis for EZH2 protein was performed on primary ATL cells, cells from healthy adults, and ATL cell lines. Primary ATL cells showed a clear 98-kDa band for EZH2 with the absence or presence of faint bands for phosphorylated EZH2 (p-EZH2). Cells from healthy adults hardly showed these bands. ATL cell lines ST1, SO4, and KK1 showed intense bands for both EZH2 and p-EZH2, but LM-Y1 and KOB cells showed intense bands for EZH2 with the absence of a band for p-EZH2. (B) Western blot analysis for histone methylation status was performed. Only primary ATL cells and LM-Y1 and KOB cell lines showed a clear band for H3K27me3, but others hardly showed the band. Bands for H3K27me2, H3K27me1, and histone H3 were observed in almost all samples examined.

with either agent alone. Similarly, cell viabilities of KOB treated with 25 nM PS (LBH589), 2.5 μ M DZNep, or a combination of these agents were 86%, 93%, and 48%, respectively. By calculating CI according to the method of Chou and Talalay,³⁹ we found a strong synergistic antiproliferative effect in both cell lines (Online Supplementary Figure S5F, lower panel).

Discussion

EZH2 is a critical component of PRC2, which mediates epigenetic gene silencing through trimethylation of H3K27.^{37,38} EED and SUZ12 are also required for the exhibition of methyltransferase activity and for the localization of this complex to target genes.³⁹ In an analysis of genome-wide H3K27 methylation in aggressive prostate cancer tissues, a significant subset of the target genes were also targets in embryonic stem cells, suggesting that the mechanism for gene silencing used to maintain stem cell renewal is converted into oncogenesis.⁴⁰ Ectopic expression of EZH2 is capable of providing a proliferative advantage to primary cells, and its gene locus is amplified in primary tumors.⁴¹ Indeed, increased EZH2 expression has been reported in several types of cancer cells, and its clinical significance is extensively studied in prostate cancer.⁴² Amounts of both *EZH2* transcript and EZH2 protein were elevated in metastatic prostate cancer; in addition, clinically localized prostate cancers that express higher concentrations of *EZH2* showed a poorer prognosis. An association of increased EZH2 expression with poor prognosis has also been reported in other solid tumors. Currently, however, there are only limited reports describing EZH2 expression in hematologic malignancies.

In the present study, we showed for the first time that EZH2 was over-expressed in ATL cells, and that the

increased EZH2 was not phosphorylated and was in its active form. The increased EZH2 seemed to exhibit histone methyltransferase activity *in vivo*, as supported by the results that ATL cells from both peripheral blood and lymph nodes were strongly positive for H3K27me3. Since EZH2 was almost undetectable in cells from healthy adults and HTLV-1 carriers, it is likely that deregulation of PRC2 caused by over-expressed EZH2 is involved in the early steps of ATL oncogenesis. Meanwhile, ATL patients with high EZH2 expression showed shorter survival than patients with low EZH2 expression, indicating that increased EZH2 also plays a role in the process of ATL progression. It has been reported that genes methylated in cancer cells are specifically packaged with nucleosomes containing H3K27.⁴³ However, there are only a few studies that actually examined H3K27me3 in primary tumor cells or tissues. In one such study, H3K27me3 expression was unexpectedly lower in breast, ovarian, and pancreatic cancers than in corresponding normal tissues, although it has been reported that there are increased levels of H3K27me3 in breast cancer cell lines.^{44,45} We do not have an adequate explanation for these conflicts at present, but there may be some differences in the process of oncogenesis between solid tumors and hematologic malignancies.

The mechanism of the overexpression of EZH2 in tumors remains largely unknown. miRNAs regulate gene expression and play important roles in cellular differentiation and embryonic stem cell development. Recently, two miRNAs, miR-101 and miR-26a, were found to repress *EZH2* expression. The expression of miR-101 decreases in parallel with an increase in *EZH2* expression during progression in prostate tumors.³⁴ In addition to these miRNAs, we examined miR-128a, which has been shown to repress *BMI1* expression in glioblastoma, because overexpression of *BMI1* is associated with the development of malignant lymphoma.^{31,36} ATL cells showed a decreased level of miR-

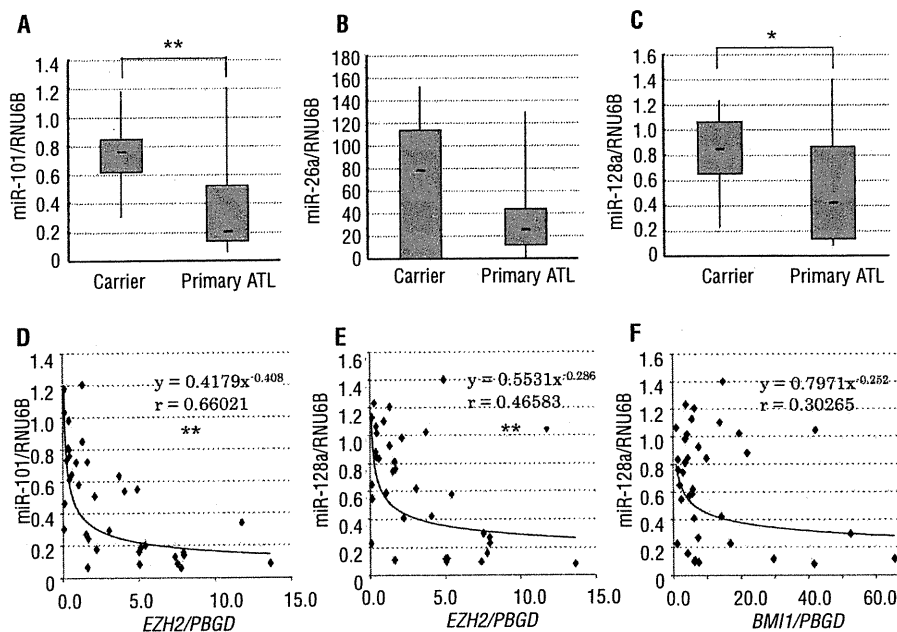


Figure 3. Quantitative real-time RT-PCR for miRNAs. (A-C) Expressions of miR-101 (A), miR-26a (B), and miR-128a (C) were compared between ATL patients and HTLV-1 carriers. Primary ATL cells showed significantly lower levels of miR-101 and miR-128a (Mann-Whitney's U test) compared with the cells from HTLV-1 carriers (A, C). There was no significant difference in miR-26a expression between the two groups (B). (D, E, F) Correlation between miRNA and *EZH2* or *BMI1* expression was examined. There were significant inverse correlations between normalized *EZH2* expression and miR-101 expression (D) or between normalized *EZH2* expression and miR-128a expression (E) (Spearman's correlation coefficient). In contrast, there was no correlation between normalized *BMI1* expression and miR-128a expression (F). * $P < 0.05$, ** $P < 0.01$.

101 expression compared with the cells from HTLV-1 carriers, which is not caused by genomic loss of the *miR-101* gene, in contrast to prostate cancer.³⁴ Moreover, there was a clear inverse correlation between *EZH2* expression and *miR-101* expression, suggesting that increased *EZH2* is caused by the decrease in *miR-101* expression. Although currently there is no report indicating an association of *miR-128a* with *EZH2* expression, *miR-128a* showed exactly the same pattern as *miR-101*, suggesting that the decrease in *miR-128a* also participates in *EZH2* overexpression in ATL. By analyzing the 3'-UTR sequence of *EZH2*, it has recently been shown that there are two predicted *miR-101* target sites and one predicted *miR-26a* target site in the 3'-UTR of *EZH2*.⁴⁶ We performed a similar analysis and found that there was also a potential target site for *miR-128a* near one of the *miR-101* target sites (Online Supplementary Figure S6). *miR-26a* was not decreased in ATL cells, and there was no correlation between *miR-26a* expression and *EZH2* expression or *miR-128a* expression and *BMI1* expression. The association of *miR-26a* with *EZH2* was found in normal cell differentiation as a physiological phenomenon but not in tumor cells. The miRNAs used to regulate normal development and differentiation may be different from those used for the development of tumors. Another possible explanation for the mechanism of increased *EZH2* expression in ATL is inactivation of *p14ARF/p15INK4B/p16INK4A* tumor suppressor genes, which frequently occurs in ATL.^{14,15,19,20} *EZH2* is a molecule downstream of the pRB-E2F pathway, and inactivation of these genes allows E2F to be released from pRB, which results in the upregulation of *EZH2* expression.⁴¹ Several recent reports indicate that *EZH2* functions to repress the expression of *p14ARF/p15INK4B/p16INK4A*; therefore, increased *EZH2* may be used to further decrease the expression of *p14ARF/p15INK4B/p16INK4A*.⁴⁷ Since somatic mutations altering *EZH2* (Tyr641) have recently been reported in follicular and diffuse large B-cell lymphomas of germinal-center origin,⁴⁸ we performed a similar analysis in 10 primary ATL samples. There were however no such mutations (Online Supplementary Figure S7).

ATL is quite resistant to antineoplastic agents and the median survival time of those with the aggressive subtypes is only 13 months, even in a recent multicenter clinical trial.⁴⁹ Since high *EZH2* expression with H3K27me3 seems

to be an essential component for the initiation and promotion of cell proliferation in ATL, we searched for the possibility of therapeutic strategies targeting *EZH2*. We examined the sensitivity of ATL cells to agents that have been shown to inhibit *EZH2* expression and histone methylation. DZNep is a carbocyclic analog of adenosine synthesized more than 20 years ago as an inhibitor of S-adenosylhomocysteine hydrolase, which has therapeutic potential as an anticancer or antiviral drug.²¹ DZNep has recently aroused interest for its unique features; it decreases the expressions of *EZH2*, *SUZ12*, and *EED* with inhibition of H3K27 methylation and induces apoptosis in cancer cells but not in normal cells.^{22,23} ATL cell lines were sensitive to DZNep and their cell proliferation was attenuated at one-tenth of the concentration used in these studies. More interestingly, DZNep showed no toxicity to normal CD4⁺ T cells as a normal control. Acute T-lymphoblastic leukemia cell lines showed similar sensitivities to DZNep, which may indicate that DZNep exerts general toxicity to leukemia and lymphoma cells not necessarily associated with histone modification. Indeed, although DZNep rather increased *EZH2* expression in KOB cells, this cell line was equally sensitive as other cell lines to DZNep. HDAC inhibitor PS (LBH589) is an effective agent for cutaneous T-cell lymphoma and induced complete remission in 2 of 9 patients involved in a phase I clinical trial.⁵⁰ More interestingly, it has been reported recently that combined use of DZNep and PS (LBH589) yielded more depletion of *EZH2* and induced more apoptosis of leukemia cells, but not normal CD34 (+) bone marrow progenitor cells.⁵¹ In the present study, we showed that the combination of DZNep and PS (LBH589) exhibited a synergistic effect in killing ATL cells. Thus, epigenetic therapy by the combined use of these agents that inhibit histone methylation could lead to a breakthrough in the treatment of aggressive ATL.

Authorship and Disclosures

The information provided by the authors about contributions from persons listed as authors and in acknowledgments is available with the full text of this paper at www.haematologica.org.

Financial and other disclosures provided by the authors using the ICMJE (www.icmje.org) Uniform Format for Disclosure of Competing Interests are also available at www.haematologica.org.

References

- Sparmann A, van Lohuizen M. Polycomb silencers control cell fate, development and cancer. *Nat Rev Cancer*. 2006;6(11):846-56.
- Lee TI, Jenner RG, Boyer LA, Guenther MG, Levine SS, Kumar RM, et al. Control of developmental regulators by Polycomb in human embryonic stem cells. *Cell*. 2006;125(2):301-13.
- Kamminga LM, Bystrykh IV, de Boer A, Houwer S, Douma J, Weersing E, et al. The Polycomb group gene *Ezh2* prevents hematopoietic stem cell exhaustion. *Blood*. 2006;107(5):2170-9.
- van Lohuizen M, Tijms M, Voncken JW, Schumacher A, Magnuson T, Wientjens E. Interaction of mouse polycomb-group (Pc-G) proteins *Enx1* and *Enx2* with *Eed*: Indication for separate Pc-G complexes. *Mol Cell Biol*. 1998;18(6):3572-9.
- Satijn DP, Hamer KM, den Blaauwen J, Otte AP. The Polycomb group protein *EED* interacts with YY1, and both proteins induce neural tissue in *Xenopus* embryos. *Mol Cell Biol*. 2001;21(4):1360-9.
- van der Vlag J, Otte AP. Transcriptional repression mediated by the human polycomb-group protein *EED* involves histone deacetylation. *Nat Genet*. 1999;23(4):474-8.
- Vire E, Brenner C, Deplus R, Blanchon L, Fraga M, Didelot C, et al. The Polycomb group protein *EZH2* directly controls DNA methylation. *Nature*. 2006;439(7078):871-4.
- Cao R, Zhang Y. The functions of *E(Z)EZH2*-mediated methylation of lysine 27 in histone H3. *Curr Opin Genet Dev*. 2004;14(2):155-64.
- Widschwendter M, Fiegl H, Egle D, Mueller-Holzner E, Spizzo G, Marth C, et al. Epigenetic stem cell signature in cancer. *Nat Genet*. 2007;39(2):157-8.
- Simon JA, Lange CA. Roles of the *EZH2* histone methyltransferase in cancer epigenetics. *Mutat Res*. 2008;647(1-2):21-9.
- Uchiyama T, Yodoi J, Sagawa K, Takatsuki K, Uchino H. Adult T-cell leukemia: clinical and hematologic features of 16 cases. *Blood*. 1977;50(3):481-92.
- Yoshida M, Seiki M, Yamaguchi K, Takatsuki K. Monoclonal integration of human T-cell leukemia provirus in all primary tumors of adult T-cell leukemia suggests causative role of human T-cell leukemia virus in the disease. *Proc Natl Acad Sci USA*. 1984;81(8):2534-7.
- Shimoyama M and members of the Lymphoma Study Group (1984-1987):

- Diagnostic criteria and classification of clinical subtypes of adult T-cell leukaemia-lymphoma. A report from the Lymphoma Study Group (1984-1987). *Br J Haematol*. 1991;79(3):428-37.
14. Hatta Y, Hiramata T, Miller CW, Yamada Y, Tomonaga M, Koeffler HP. Homozygous deletions of p15 (MTS2) and p16 (CDKN2/MTS1) genes in adult T-cell leukemia. *Blood*. 1995;85(10):2699-704.
 15. Yamada Y, Hatta Y, Murata K, Sugawara K, Ikeda S, Mine M, et al. Deletions of p15 and/or p16 genes as a poor-prognosis factor in adult T-cell leukemia. *J Clin Oncol*. 1997;15(5):1778-85.
 16. Nagai H, Kinoshita T, Imamura J, Murakami Y, Hayashi K, Mukai K, et al. Genetic alteration of p53 in some patients with adult T-cell leukemia. *Jpn J Cancer Res*. 1991;82(12):1421-7.
 17. Sakashita A, Hattori T, Miller CW, Suzushima H, Asou N, Takatsuki K, et al. Mutations of the p53 gene in adult T-cell leukemia. *Blood*. 1992;79(2):477-80.
 18. Tawara M, Hogerzeil SJ, Yamada Y, Takasaki Y, Soda H, Hasegawa H, et al. Impact of p53 aberration on the progression of adult T-cell leukemia/lymphoma. *Cancer Lett*. 2006;234(2):249-55.
 19. Kohno T, Yamada Y, Tawara M, Takasaki Y, Kamihira S, Tomonaga M, et al. Inactivation of p14ARF as a key event for the progression of adult T-cell leukemia/lymphoma. *Leuk Res*. 2007;31(12):1625-32.
 20. Nosaka K, Maeda M, Tamiya S, Sakai T, Mitsuya H, Matsuo M. Increasing methylation of the CDKN2A gene is associated with the progression of adult T-cell leukemia. *Cancer Res*. 2000;60(4):1043-8.
 21. Glazer RI, Hartman KD, Knode MC, Richard MM, Chiang PK, Tseng CK, et al. 3-Deazaneplanocin: a new and potent inhibitor of S-adenosylhomocysteine hydrolase and its effects on human promyelocytic leukemia cell line HL-60. *Biochem Biophys Res Commun*. 1986;135(2):688-94.
 22. Miranda TB, Cortez CC, Yoo CB, Liang G, Abe M, Kelly TK, et al. DZNep is a global histone methylation inhibitor that reactivates developmental genes not silenced by DNA methylation. *Mol Cancer Ther*. 2009;8(6):1579-88.
 23. Tan J, Yang X, Zhuang L, Jiang X, Chen W, Lee PL, et al. Pharmacologic disruption of Polycomb-repressive complex 2-mediated gene repression selectively induces apoptosis in cancer cells. *Genes Dev*. 2007;21(9):1050-63.
 24. Fiskus W, Pranpat M, Balasis M, Herger B, Rao R, Chinniyar A, et al. Histone deacetylase inhibitors deplete EZH2 and associated Polycomb Repressive Complex 2 proteins with attenuation of HOXA9 and MEIS1 and loss of survival of human acute leukemia cells. *Mol Cancer Ther*. 2006;5(12):3096-104.
 25. Choi YL, Tsukasaki K, O'Neill MC, Yamada Y, Onimaru Y, Matsumoto K, et al. A genomic analysis of adult T-cell leukemia. *Oncogene*. 2007;26(8):1245-55.
 26. Yamada Y, Ohmoto Y, Hata T, Yamamura M, Murata K, Tsukasaki K, et al. Features of the cytokines secreted by adult T cell leukemia (ATL) cells. *Leuk Lymphoma*. 1996;21(5-6):443-7.
 27. Choi YL, Makishima H, Ohashi J, Yamashita Y, Ohki R, Koinuma K, et al. DNA microarray analysis of natural killer cell-type lymphoproliferative disease of granular lymphocytes with purified CD3(-) CD56(+) fractions. *Leukemia*. 2004;18(3):556-65.
 28. Hasegawa H, Yamada Y, Komiyama K, Hayashi M, Ishibashi M, Sunazuka T, et al. A novel natural compound, a cycloanthranilylproline derivative (Fuligocandin B), sensitizes leukemia cells to apoptosis induced by tumor necrosis factor related apoptosis-inducing ligand (TRAIL) through 15-deoxy-Delta 12,14 prostaglandin J2 production. *Blood*. 2007;110(5):1664-74.
 29. Chou TC, Talalay P. Quantitative analysis of dose-effect relationships: the combined effects of multiple drugs or enzyme inhibitors. *Adv Enzyme Regul*. 1984;22:27-55.
 30. Yasunaga J, Taniguchi Y, Nosaka K, Yoshida M, Satou Y, Sakai T, et al. Identification of aberrantly methylated genes in association with adult T-cell leukemia. *Cancer Res*. 2004;64(17):6002-9.
 31. Jacobs JJ, Kieboom K, Marino S, DePinho RA, van Lohuizen M. The oncogene and Polycomb-group gene bmi-1 regulates cell proliferation and senescence through the ink4a locus. *Nature*. 1999;397(6715):164-8.
 32. Scott CL, Gil J, Hernandez E, Teruya-Feldstein J, Narita M, Martinez D, et al. Role of the chromobox protein CBX7 in lymphomagenesis. *Proc Natl Acad Sci USA*. 2007;104(13):5389-94.
 33. Cha TL, Zhou BF, Xia W, Wu Y, Yang CC, Chen CT, et al. Akt-mediated phosphorylation of EZH2 suppresses methylation of Lysine 27 in histone H3. *Science*. 2005;310(5746):306-10.
 34. Varambally S, Cao Q, Mani RS, Shankar S, Wang X, Ateeq B, et al. Genomic loss of microRNA-101 leads to overexpression of histone methyltransferase EZH2 in cancer. *Science*. 2008;322(5908):1695-6.
 35. Sander S, Bullinger L, Klapproth K, Fiedler K, Kestler HA, Barth TF, et al. MYC stimulates EZH2 expression by repression of its negative regulator miR-26a. *Blood*. 2008;112(10):4202-12.
 36. Godlewski J, Nowicki MO, Bronisz A, Williams S, Otsuki A, Nuovo G, et al. Targeting of the Bmi-1 oncogene/stem cell renewal factor by microRNA-128 inhibits glioma proliferation and self-renewal. *Cancer Res*. 2008;68(22):9125-30.
 37. Cao R, Wang L, Wang H, Xia L, Erdjument-Bromage H, Tempst P, et al. Role of histone H3 lysine 27 methylation in Polycomb-group silencing. *Science*. 2002;298(5595):1039-43.
 38. Czermin B, Melfi R, McCabe D, Seitz V, Imhof A, Pirrotta V. Drosophila enhancer of Zeste/ESC complexes have a histone H3 methyltransferase activity that marks chromosomal Polycomb sites. *Cell*. 2002;111(2):185-96.
 39. Cao R, Zhang YL. SUZ12 is required for both the histone methyltransferase activity and the silencing function of the EED-EZH2 complex. *Mol Cell*. 2004;15(1):57-67.
 40. Yu J, Yu J, Rhodes DR, Tomlins SA, Cao X, Chen G, et al. A polycomb repression signature in metastatic prostate cancer predicts cancer outcome. *Cancer Res*. 2007;67(22):10657-63.
 41. Bracken AP, Pasini D, Capra M, Prosperini E, Colli E, Helin K. EZH2 is down stream of the pRB-E2F pathway, essential for proliferation and amplified in cancer. *EMBO J*. 2003;22(20):5323-35.
 42. Varambally S, Dhanasekaran SM, Zhou M, Barrette TR, Kumar-Sinha C, Sanda MG, et al. The polycomb group protein EZH2 is involved in progression of prostate cancer. *Nature*. 2002;419(6907):624-9.
 43. Schlesinger Y, Straussman R, Keshet I, Farkash S, Hecht M, Zimmerman J, et al. Polycomb-mediated methylation of Lys27 of histone H3 pre-marks genes for de novo methylation in cancer. *Nat Genet*. 2007;39(2):232-6.
 44. Wei Y, Xia W, Zhang Z, Liu J, Wang H, Adsay NV, et al. Loss of trimethylation at lysine 27 of histone H3 is a predictor of poor outcome in breast, ovarian, and pancreatic cancers. *Mol Carcinog*. 2008;47(9):701-6.
 45. Sun F, Chan E, Wu Z, Yang X, Marquez VE, Yu Q. Combinatorial pharmacologic approaches target EZH2-mediated gene repression in breast cancer cells. *Mol Cancer Ther*. 2009;8(12):3191-202.
 46. Cao P, Deng Z, Wan M, Huang W, Cramer SD, Xu J, et al. MicroRNA-101 negatively regulates Ezh2 and its expression is modulated by androgen receptor and HIF-1alpha/HIF-1beta. *Mol Cancer*. 2010;9:108.
 47. Bracken AP, Kleene-Kohlbrecher D, Dietrich N, Pasini D, Gargiulo G, Beekman C, et al. The polycomb group proteins bind throughout the INK4A-ARF locus and are disassociated in senescent cells. *Genes Dev*. 2007;21(5):525-30.
 48. Morin RD, Johnson NA, Severson TM, Mungall AJ, An J, Goya R, et al. Somatic mutations altering EZH2 (Tyr641) in follicular and diffuse large B-cell lymphomas of germinal-center origin. *Nat Genet*. 2010;42(2):181-5.
 49. Yamada Y, Tomonaga M, Fukuda H, Hanada S, Utsunomiya A, Tara M, et al. A new G-CSF-supported combination chemotherapy, LSG15, for adult T-cell leukaemia-lymphoma: Japan Clinical Oncology Group Study 9303. *Br J Haematol*. 2001;113(2):375-82.
 50. Ellis L, Pan Y, Smyth GK, George DJ, McCormack C, Williams-Truax R, et al. Histone deacetylase inhibitor panobinostat induces clinical responses with associated alterations in gene expression profiles in cutaneous T-cell lymphoma. *Clin Cancer Res*. 2008;14(14):4500-10.
 51. Fiskus W, Wang Y, Sreekumar A, Buckley KM, Shi H, Jillella A, et al. Combined epigenetic therapy with the histone methyltransferase EZH2 inhibitor 3-deazaneplanocin A and the histone deacetylase inhibitor panobinostat against human AML cells. *Blood*. 2009;114(13):2733-43.

blood

2011 118: 6881-6892
Prepublished online October 31, 2011;
doi:10.1182/blood-2011-05-354654

miR-135b mediates NPM-ALK-driven oncogenicity and renders IL-17-producing immunophenotype to anaplastic large cell lymphoma

Hironori Matsuyama, Hiroshi I. Suzuki, Hikaru Nishimori, Masaaki Noguchi, Takashi Yao, Norio Komatsu, Hiroyuki Mano, Koichi Sugimoto and Kohei Miyazono

Updated information and services can be found at:

<http://bloodjournal.hematologylibrary.org/content/118/26/6881.full.html>

Articles on similar topics can be found in the following Blood collections
Lymphoid Neoplasia (1027 articles)

Information about reproducing this article in parts or in its entirety may be found online at:
http://bloodjournal.hematologylibrary.org/site/misc/rights.xhtml#repub_requests

Information about ordering reprints may be found online at:
<http://bloodjournal.hematologylibrary.org/site/misc/rights.xhtml#reprints>

Information about subscriptions and ASH membership may be found online at:
<http://bloodjournal.hematologylibrary.org/site/subscriptions/index.xhtml>

Blood (print ISSN 0006-4971, online ISSN 1528-0020), is published weekly by the American Society of Hematology, 2021 L St, NW, Suite 900, Washington DC 20036.
Copyright 2011 by The American Society of Hematology; all rights reserved.



miR-135b mediates NPM-ALK-driven oncogenicity and renders IL-17-producing immunophenotype to anaplastic large cell lymphoma

*Hironori Matsuyama,¹ *Hiroshi I. Suzuki,¹ Hikaru Nishimori,¹ Masaaki Noguchi,² Takashi Yao,³ Norio Komatsu,⁴ Hiroyuki Mano,^{5,6} Koichi Sugimoto,⁴ and Kohei Miyazono¹

¹Department of Molecular Pathology, Graduate School of Medicine, University of Tokyo, Tokyo, Japan; ²Department of Hematology, Juntendo Urayasu Hospital, Chiba, Japan; ³Department of Human Pathology and ⁴Division of Hematology, Department of Internal Medicine, Juntendo University School of Medicine, Tokyo, Japan; ⁵Department of Medical Genomics, Graduate School of Medicine, University of Tokyo, Tokyo, Japan; and ⁶Division of Functional Genomics, Jichi Medical University, Tochigi, Japan

Many transformed lymphoma cells show immune-phenotypes resembling the corresponding normal lymphocytes; thus, they provide a guide for proper diagnosis and present promising routes to improve their pathophysiologic understanding and to identify novel therapeutic targets. However, the underlying molecular mechanism(s) of these aberrant immune-phenotypes is largely unknown. Here, we report that microRNA-135b (miR-135b) mediates nucleophosmin-anaplastic lymphoma kinase (NPM-ALK)-driven oncogenicity and empowers IL-17-producing immunophenotype in anaplastic large cell

lymphoma (ALCL). NPM-ALK oncogene strongly promoted the expression of miR-135b and its host gene LEMD1 through activation of signal transducer and activator of transcription (STAT) 3. In turn, elevated miR-135b targeted FOXO1 in ALCL cells. miR-135b introduction also decreased chemosensitivity in Jurkat cells, suggesting its contribution to oncogenic activities of NPM-ALK. Interestingly, miR-135b suppressed T-helper (Th) 2 master regulators STAT6 and GATA3, and miR-135b blockade attenuated IL-17 production and paracrine inflammatory response by ALCL cells, indicating that miR-135b-

mediated Th2 suppression may lead to the skewing to ALCL immunophenotype overlapping with Th17 cells. Furthermore, antisense-based miR-135b inhibition reduced tumor angiogenesis and growth in vivo, demonstrating significance of this "Th17 mimic" pathway as a therapeutic target. These results collectively illuminated unique contribution of oncogenic kinase-linked microRNA to tumorigenesis through modulation of tumor immune-phenotype and microenvironment. (*Blood*. 2011;118(26):6881-6892)

Introduction

MicroRNAs (miRNAs) are endogenous noncoding, 20- to 23-nucleotide single-stranded RNAs that negatively regulate gene expression in a sequence-specific manner.¹ miRNA species are generated through RNase-mediated processing reaction by two central RNases III, Drosha and Dicer, from long primary transcripts (primary miRNAs [pri-miRNAs]) and incorporated along with core Argonaute proteins into the RNA-induced silencing complex. RNA-induced silencing complex interacts mainly with 3' untranslated region (UTR) of target mRNAs through partial base complementarity to the 5' miRNA seed region, leading to degradation, destabilization, or translational inhibition of target mRNAs. miRNAs regulate differentiation and functions of various cell types, including immune cells in a highly context-dependent manner.²

Alteration of miRNome has emerged as a key feature of cancer-associated dysfunction of gene regulatory networks. Although miRNA dysregulation affects cancer cell behavior with other genetic and epigenetic abnormalities, full pictures of their causes and consequences remain to be elucidated.³ In hematologic malignancies, many transformed lymphoma cells show immune-phenotypes resembling the corresponding normal lymphocytes; thus, they represent a guide for proper diagnosis and promising routes to improve our understanding of their pathogenesis and to identify novel therapeutic targets.⁴ For example, diffuse large

B-cell lymphomas have been shown to be composed of at least 2 prognostic entities, depending on its resemblance to normal germinal center or activated B cells.⁵ However, the molecular basis shaping the aberrant immunophenotypes of tumor cells has been largely unknown, and the relationship between miRNA regulation and lymphoma phenotype has not been investigated.

Recent studies revealed several mechanisms regulating miRNA expression.⁶ Although certain oncoproteins, including Myc and tumor suppressors such as p53, have been linked to the regulation of miRNA expression,^{7,8} involvement of oncogenic tyrosine kinases remains unclear in this regulatory pathway. Anaplastic lymphoma kinase (ALK) exerts characteristic oncogenic activities through fusion to several gene partners or mutations both in hematopoietic and nonhematopoietic solid tumors.^{9,10} Nucleophosmin (NPM)-ALK is a representative translocation-dependent fusion-type oncogenic tyrosine kinase in anaplastic large cell lymphoma (ALCL). Although NPM-ALK drives malignant transformation of ALCL cells through various molecular mechanisms, including activation of signal transducer and activator of transcription (STAT) 3, Ras-ERK, and PI3K oncogenic signaling pathways,⁹ involvement of miRNAs has not been reported so far. Here, we have explored unrecognized involvement of miRNAs in the downstream of NPM-ALK.

Submitted May 12, 2011; accepted October 25, 2011. Prepublished online as *Blood* First Edition paper, October 31, 2011; DOI 10.1182/blood-2011-05-354654.

*H.M. and H.I.S. contributed equally to this study.

The online version of the article contains a data supplement.

The publication costs of this article were defrayed in part by page charge payment. Therefore, and solely to indicate this fact, this article is hereby marked "advertisement" in accordance with 18 USC section 1734.

© 2011 by The American Society of Hematology

We identified miR-135b as one of the major downstream executors of NPM-ALK chimeric oncoprotein in ALCL. NPM-ALK strongly promoted the expression of miR-135b and its host gene LEMD1 through STAT3 activation. The elevated miR-135b targeted FOXO1 tumor suppressor. Interestingly, we further revealed the immune modulatory property of miR-135b shaping the T-cell phenotypes of ALCL cells. miR-135b suppressed T-helper (Th) 2 master regulators STAT6 and GATA3, and the blockade of miR-135b attenuated IL-17 production and paracrine inflammatory response by ALCL cells, suggesting that miR-135b-mediated Th2 suppression may skew the ALCL immunophenotype to overlap with that of Th17 cells. Antisense-based miR-135b inhibition reduced tumor angiogenesis and growth in vivo, underscoring the pathogenic roles of this pathway. Our findings revealed that miR-135b is involved in NPM-ALK-driven tumorigenesis and modulation of ALCL immunophenotype, and they also suggest dynamic commitment of miRNAs to mutual regulation between Th cell differentiation programs and determination of polarized immunophenotypes of malignant cells.

Methods

Cell lines and reagents

Karpas 299, SUDHL-1, and SUP-M2 cell lines were obtained from the German Collection of Microorganisms and Cell Cultures. Jurkat, Molt4, CCRF-CEM, HCT116, HEK293T, HeLa, and lung cancer cell lines were obtained from the American Type Culture Collection. WI-38 human diploid fibroblast line was obtained from the RIKEN Cell Bank. Human normal peripheral blood pan T lymphocytes were purchased from AllCells. Neuroblastoma cell lines were kindly provided from R. Sakai (National Cancer Center Research Institute, Tokyo, Japan). Hematologic, neuroblastoma, and lung cancer cell lines were maintained in RPMI-1640 (Invitrogen) containing 10% FBS, 100 units/mL penicillin, and 100 µg/mL streptomycin. Other cell lines were maintained in Dulbecco modified eagle medium (Invitrogen) with 10% FBS. In coculture experiment, Karpas 299 and WI-38 cells were cocultured (in Opti-MEM [Invitrogen] with 1% FBS) for 48 hours using Transwell tissue culture inserts (0.4-µm pore size; BD Biosciences). The following antibodies were used: ALK 4CSB8 (Invitrogen); STAT3 124H6, p-STAT3 D3A7, Akt 9272, p-Akt 193H12, FOXO1 C29H4, and STAT6 9362 (Cell Signaling Technology); p21 H-164, p27 F-8, and GATA3 HG3-31 (Santa Cruz Biotechnology); CREG1 299133 (R&D Systems); CD31 555024 (BD Biosciences); and α -tubulin DM-1A (Sigma-Aldrich). Kinase inhibitors (WHI-P154, U0126 and LY294002) were purchased from Calbiochem.

Patient samples

ALCL patients were diagnosed at Juntendo University Hospital and Juntendo Urayasu Hospital. Investigations were carried out in accordance with ethical standards authorized by the ethics committees of University of Tokyo, Juntendo University School of Medicine, and Jichi Medical University. Written informed consent was obtained in accordance with the Declaration of Helsinki.

TuD miRNA system, shRNA, and plasmids

Tough decoy RNA (TuD RNA) against miR-135b was designed according to a previous report.¹¹ Detailed structures of TuD RNA are described in supplemental Table 1 (available on the *Blood* Web site; see the Supplemental Materials link at the top of the online article). shRNAs were designed as described previously.^{12,13} TuD RNAs and shRNAs were introduced into pENTR-H1 vector. Pri-miRNA expression vectors were generated by cloning short fragments of pri-miRNAs containing pre-miRNA and flanking sequence on both sides of pre-miRNA into pcDNA6.2-GW/EmGFP-miR (Invitrogen). miRNA sensor vectors were prepared by inserting mature

miRNA complementary sequences within the XhoI and NotI sites of the 3'UTR of the luciferase gene in the Psicheck 2 dual luciferase reporter vector (Promega). For other reporter constructs, the 3'UTR segment of each target gene was cloned into the same luciferase reporter vector. The primer sequences used are given in supplemental Table 2. For transient transfection, pre-miRNA precursors (Ambion) also were used.

Luciferase reporter assay

Cells were transfected with each reporter construct with pri-miRNA expression vector using Lipofectamine 2000 (Invitrogen). Cell extracts were prepared 24 to 48 hours after transfection, and the ratio of *Renilla* to firefly luciferase was measured using the Dual-Luciferase Reporter Assay System (Promega).

qRT-PCR assays

Quantitative (q)RT-PCR assays were performed as described previously.⁸ For detection of mRNAs, total RNA was extracted by TRIzol (Invitrogen) and subjected to reverse transcription using the PrimeScriptII first-strand cDNA synthesis kit (Takara) according to the manufacturer's instructions. qRT-PCR was performed with the 7500 Fast Real-Time PCR System (Applied Biosystems). The expression levels of mature miRNAs were determined using TaqMan MicroRNA assay kit (Applied Biosystems) according to the manufacturer's protocol. Data analysis was done by the comparative C_T method. Results were normalized to β -actin for pri-miRNA detection, and RNU44 small nucleolar RNA for evaluation of mature miRNA. miRNeasy mini kit (QIAGEN) or RecoverAll total nucleic acid isolation kit for FFPE Tissues (Ambion) was used for RNA extraction from clinical samples. The primer sequences used are given in supplemental Table 3.

Chromatin immunoprecipitation analysis

Cells were fixed by adding formaldehyde and then harvested. After sonication, samples were incubated at 4°C overnight with protein A or anti-mouse IgG-Dynabeads that had been preincubated with 5 to 10 µg of antibodies in PBS and 0.5% BSA. To precipitate STAT3, anti-STAT3 antibody 124H6 (Cell Signaling Technology) was used. Immunoprecipitated samples were eluted and reverse-crosslinked by incubation overnight at 65°C. Genomic DNA was then extracted with a PCR purification kit (QIAGEN) and subjected to PCR analysis. The primer sequences used are given in supplemental Table 3.

Lentiviral gene transfer

TuD RNAs, shRNAs, pri-miRNA, NPM-ALK, or mouse constitutively active (ca)-STAT3 (A662C/N664C)¹⁴ was introduced by lentiviral infection system (a kind gift from H. Miyoshi, RIKEN, Tsukuba, Japan). TuD RNAs and shRNAs were transferred into lentivirus vector CS-RfA-EG via pENTR-H1 vector using LR clonase. Pri-miRNA was similarly transferred into CSII-EF-RfA-CMV-Puro lentivirus vector using pENTR vector. The lentivirus production was carried out by transfection of HEK293FT cells with the vector construct pCMV-VSV-G-RSV-Rev and pCAG-HIVgp. The viral particles were collected 48 hours after transfection, titered by Lenti-X qRT-PCR titration kit (Takara), introduced to cultured cells, and monitored by flow cytometric analysis to determine infection efficiency.

Immunoblot assay

Cells were lysed with a buffer containing 1% Nonidet P-40, 20mM Tris-HCl, pH 7.4, 150mM NaCl, 5mM EDTA, and 1% protease inhibitor mixture (Nacalai Tesque). Total cell lysates were subjected to SDS-PAGE and transferred to Fluoro Trans W membrane (Pall). Immunoblotting was performed using the indicated antibodies.

Drug sensitivity assay

Jurkat cells were seeded at a density of 1×10^5 /mL and split 24 hours before treatment. After 24-hour treatment with different concentrations of cytosine β -D-arabinofuranoside (Sigma-Aldrich), cells were collected,

washed, and reseeded for assay of cell viability and apoptosis. Cell viability and apoptosis were assessed by WST-8 colorimetric assay (Nacalai Tesque) and annexin V assay kit (BD Biosciences), respectively.

ELISA

After transfection with miRCURY LNA microRNA power inhibitor (EXIQON; Control A or antisense against miR-135b), IL-17F concentrations in the culture supernatant (72 hours) of Karpas 299 cells were determined by ELISA kit (R&D Systems; DuoSet human IL17F), according to the manufacturer's instructions.

In vivo cancer models

C.B-17/IcrCrj severe combined immunodeficient (SCID) female mice (4 weeks of age) were obtained from Charles River Japan. All animal experimental protocols were performed in accordance with the policies of the Animal Ethics Committee of the University of Tokyo. Karpas 299 cells (1×10^6 ; $n = 6/\text{group}$) were subcutaneously injected in 0.2 mL of a mixture of RPMI-1640 without FBS and 30% Matrigel (BD Biosciences) into female SCID mice and allowed to grow for 1 week to reach a volume of 50 to 200 mm³. Complexes of miRCURY LNA microRNA power inhibitor (EXIQON; Control A or antisense against miR-135b) and atelocollagen (Koken) were prepared according to the manufacturer's instructions. Antisense oligonucleotides (5 μM) with atelocollagen in a 200- μL volume were administered into the subcutaneous spaces around the tumors at days 7 and 10 after inoculation. Subcutaneous xenografts were measured externally every day until the end of evaluation periods, and tumor volume was approximated using the equation $\text{vol} = (a \times b^2)/2$, where vol is volume, a the length of the major axis, and b the length of the minor axis.

Immunohistochemistry

Tumor samples excised from the animals were fixed for 1 hour in 10% neutral-buffered formalin at room temperature, washed overnight in PBS containing 10% sucrose at 4°C, and embedded in optimal cutting temperature compound (Tissue-Tek). The samples were then snap-frozen in dry-iced acetone for immunohistochemistry. Frozen samples were further sectioned at 10- μm thickness in a cryostat, briefly fixed with 10% formalin, and then incubated with primary and secondary antibodies. Samples were observed using an LSM510 Meta confocal microscope (Carl Zeiss). Quantification of CD31-stained areas was performed in multiple fields on tumor sections from 6 mice using Photoshop 8.0.1 software (Adobe Systems) and ImageJ 1.36b software (National Institutes of Health).

GEP analysis

Microarray data for NPM-ALK gene expression signature (GSE6184) and clinical gene expression profiling (GEP) data of peripheral T-cell lymphoma (PTCL) patient samples (GSE19069) were obtained from the National Center for Biotechnology Information's Gene Expression Omnibus.^{12,15} Gene-set enrichment analysis (GSEA) was performed with GSEA Version 2.0 software available from the Broad Institute (<http://www.broadinstitute.org/gsea/>) using microarray data for NPM-ALK signature (GSE6184) and GSEA-embedded potential miRNA target gene sets or TargetScan-predicted putative miRNA target lists (<http://www.targetscan.org/>).¹⁶

Statistical analysis

Statistical analysis was performed using the Student t test or multivariate ANOVA (for proliferation assay and in vivo analysis; * $P < .05$; ** $P < .01$; *** $P < .001$). All data are expressed as mean \pm SEM.

Results

Up-regulation of miR-135b in ALCL

Previous microarray analysis on miRNA expression identified various signatures of aberrant miRNA expression in a wide range

of hematologic cell lines, including major types of B- and T-cell lymphoma, lymphoproliferative disorder, T-cell acute lymphoblastic leukemia, and acute myeloid leukemia.¹⁷ In this analysis, ALCL was characterized by increased expression of miR-135b, miR-21, and miR-27a.¹⁷ We verified the observation using quantitative RT-PCR analysis on 3 ALCL cell lines carrying *NPM-ALK* fusion; Karpas 299, SUDHL-1, and SUP-M2 (Figure 1A-C). Among these miRNAs, miR-135b was most prominently up-regulated in ALCL cell lines, and it was reduced by the ALK inhibitor WHI-P154 (Figure 1D), prompting us to track potential downstream effector(s) of NPM-ALK to miR-135b. Because miR-135b is located in the first intron of the LEM domain containing 1 (*LEMD1*) gene on 1q32.1 (Figure 1E), we examined *LEMD1* expression levels in ALCL cell lines. *LEMD1* was also remarkably elevated in ALCL cells (Figure 1F). ALK inhibition resulted in a potent decrease of *LEMD1* and primary transcript of miR-135b (pri-miR-135b) in Karpas 299 and SUDHL-1 cells (Figure 1G), as well as in mature miR-135b, suggesting that NPM-ALK characterizes high miR-135b expression in ALCL cells. The effects of WHI-P154 on mature miR-135b were lower than those on pri-miR-135b, possibly because of generally high stability of mature miRNAs. In addition, we measured miR135b expression levels in clinical samples of ALCL patients and found that miR-135b is elevated in human primary ALK-positive ALCL samples, compared with reactive lymph node and ALK-negative ALCL samples (Figure 1H).

NPM-ALK induces *LEMD1*/miR-135b through STAT3 activation

To examine a direct involvement of NPM-ALK in miR-135b up-regulation in ALCL cells, we introduced wild-type and kinase-dead NPM-ALK into the human Jurkat cells and examined the expression levels of *LEMD1* and miR-135b. NPM-ALK but not kinase-dead NPM-ALK (K210R) induced both *LEMD1* and mature miR-135b in Jurkat cells (Figure 2A), indicating that NPM-ALK up-regulates the host gene and subsequently miR-135b through the kinase activity.

Because previous reports demonstrated that NPM-ALK elicits many downstream pathways, including STAT3, Ras-ERK, and PI3K signaling pathways,⁹ we next examined the involvement of these pathways. Knockdown of NPM-ALK or STAT3 suppressed the expression of *LEMD1* and miR-135b in ALCL cells (Figure 2B and supplemental Figure 1A),^{12,13} whereas inhibition of ERK or PI3K failed to exert such effects (supplemental Figure 1B). We also confirmed that ca-STAT3 up-regulates *LEMD1* and miR-135b in Jurkat cells (Figure 2C). Furthermore, we analyzed putative STAT3-binding sites within the conserved region of *LEMD1* gene between human and mouse and showed that STAT3 binds to putative STAT3-binding sites within the *LEMD1* genomic region by chromatin-immunoprecipitation analysis (Figure 2D-E). Reflecting high miR-135b expression, luciferase expression levels from miR-135b sensor vector were remarkably lower than those from control sensor vector in ALCL cells but not in Jurkat cells, confirming that miR-135b is highly active in ALCL cells (Figure 2F). Taken together, these results demonstrate that miR-135b lies downstream of the NPM-ALK/STAT3 signaling pathway in ALCL.

miR-135b targets FOXO1 and regulates chemosensitivity

Several potential targets of miR-135b with tumor-suppressive activities were computationally predicted previously¹⁸ and included APC, LZTS1, LZTS2, CREG1, and FOXO1. APC has been already shown as a target of miR-135b,¹⁹ and we validated LZTS1, LZTS2, and FOXO1 using luciferase reporter assay (supplemental

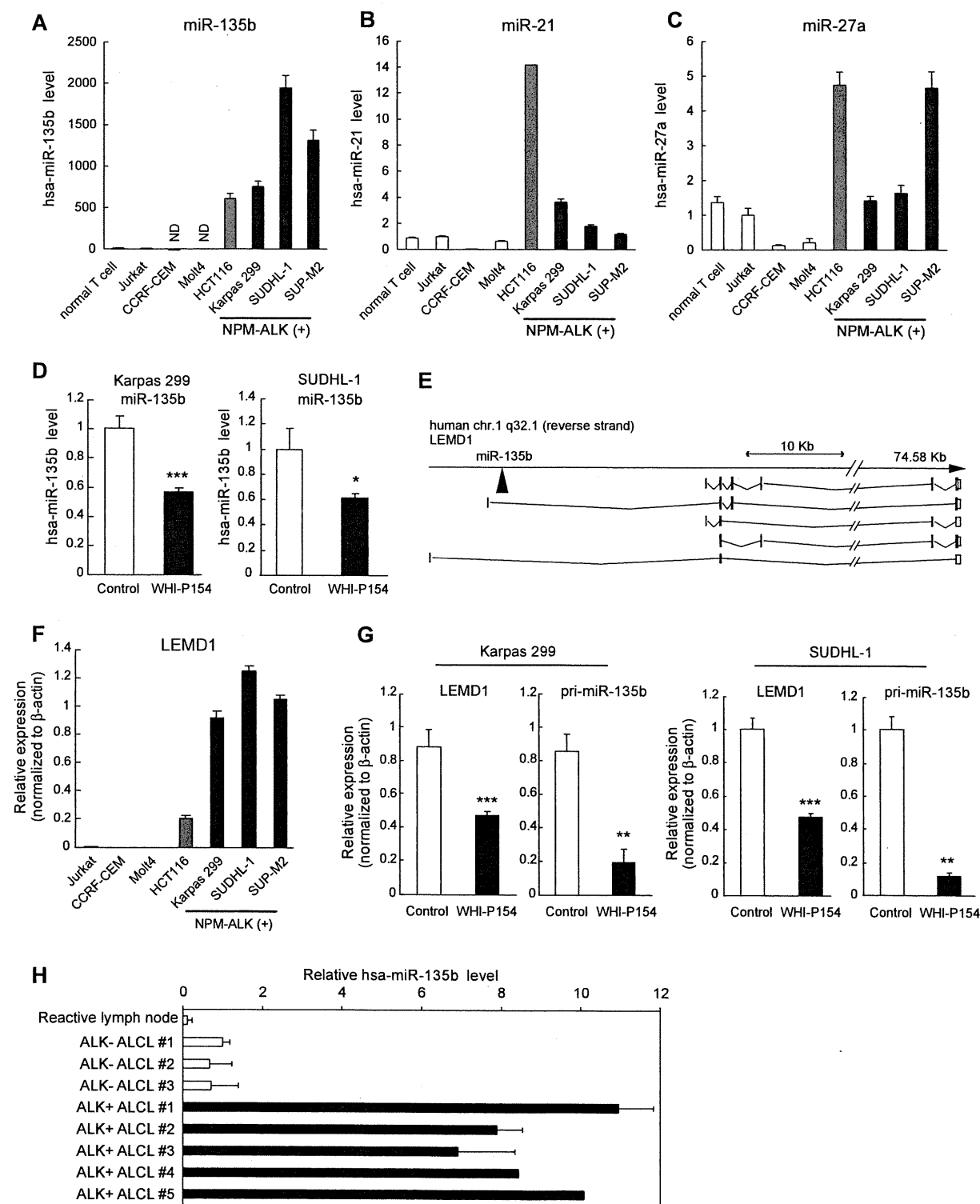


Figure 1. High expression of miR-135b and LEMD1 in ALCL. (A-C) Expression of mature miR-135b (A), miR-21 (B), and miR-27a (C) in NPM-ALK (+) ALCL cell lines (Karpas 299, SUDHL-1, and SUP-M2), normal T lymphocytes, and several T-lymphoblastic leukemia cell lines (Jurkat, CCRF-CEM, and Molt4), detected by qRT-PCR analysis. HCT116 colon cancer cells expressing endogenous miR-135b were used as positive control. ND indicates not detected. (D) Attenuation of miR-135b expression by ALK inhibitor WHI-P154. Mature miR-135b in Karpas 299 and SUDHL-1 cells was analyzed by qRT-PCR after WHI-P154 treatment (10 μ M, 4 hours). (E) Schematic diagram of genomic organization of human *LEMD1* gene and miR-135b. As for human *LEMD1*, several splicing variants have been reported. miR-135b is located in the first intron of *LEMD1* longer transcripts. (F) High expression of LEMD1 in ALCL cells, determined as in panel A. (G) Suppression of LEMD1 and pri-miR-135b by WHI-P154 (10 μ M, 1 hour) in Karpas 299 and SUDHL-1 cells, assessed as in panel D (* P < .05; ** P < .01; *** P < .001). (H) Expression of miR-135b in clinical samples of ALCL patients.

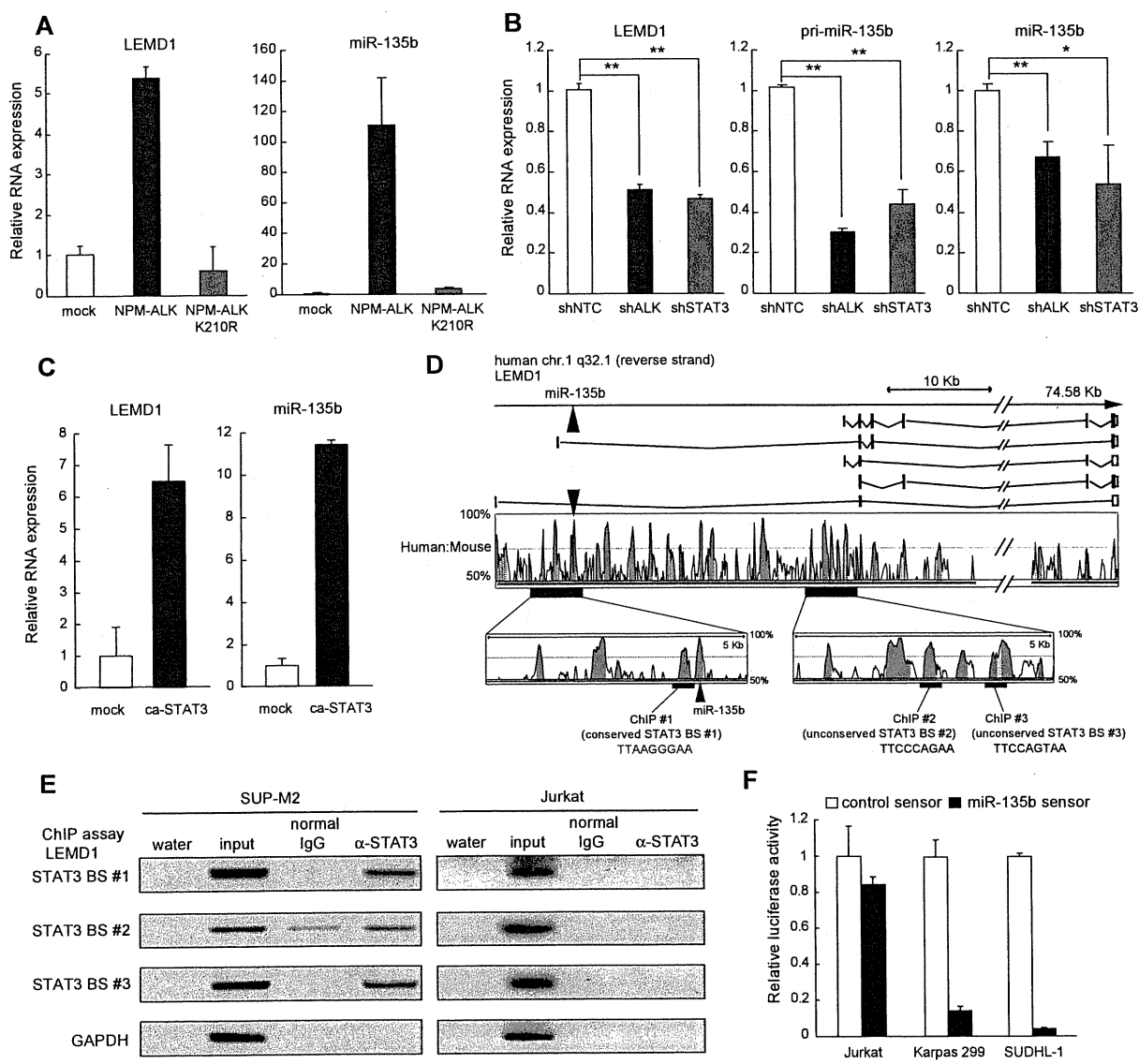


Figure 2. Identification of NPM-ALK-STAT3-miR-135b axis in ALCL. (A) Induction of LEMD1/miR-135b by NPM-ALK. Jurkat cells were transduced with lentivirus carrying NPM-ALK or kinase-dead NPM-ALK (K210R) and subjected to qRT-PCR analysis. (B) NPM-ALK/STAT3-dependent up-regulation of LEMD1/miR-135b in ALCL. Effects of shRNAs against NPM-ALK and STAT3 were evaluated in SUDHL-1 cells (* $P < .05$; ** $P < .01$). (C) Up-regulation of LEMD1/miR-135b by ca-STAT3. Jurkat cells were transduced with lentivirus carrying mouse ca-STAT3 and subjected to qRT-PCR analysis. (D) STAT3 binding sites in *LEMD1* genomic region. Top panel indicates schematic genomic organization of human *LEMD1* gene and miR-135b. Sequence conservation between human and mouse is represented as the percentage of conservation in the Vista analysis shown in the middle panel. We analyzed putative STAT3-binding sites within the conserved region in ChIP analysis, and we found that STAT3 bound to 3 sites in the bottom panel, as shown in panel E. Number 1 site (TTAAGGGAA) is conserved between human and mouse. (E) Binding of STAT3 to *LEMD1* genomic regions analyzed by ChIP analysis in SUP-M2 (left) and Jurkat (right) cells. Total chromatin before immunoprecipitation was used as positive control for PCR. Jurkat cells were used as negative control. (F) Enhanced miR-135b activity in ALCL. Cells were transfected with miRNA sensor vectors and applied to luciferase assay. Reflecting high miR-135b expression, luciferase expression levels from miR-135b sensor vector were remarkably lower than those from control sensor vector in ALCL cells but not in Jurkat cells.

Figure 2A-B). To identify the endogenous and functional target(s) of miR-135b in ALCL cells, we achieved the efficient long-term suppression of miR-135b activity through the decoy RNA system, in which RNA decoys against specific miRNA (TuD RNA) are driven by RNA polymerase III (Figure 3A).¹¹ Introduction of TuD RNA indeed strongly inhibited miR-135b activity in ALCL cell lines (Figure 3B-C and supplemental Figure 2C-D).

Using this system, we consequently identified FOXO1 as an endogenous target of miR-135b in ALCL (Figure 3D-G). The FOXO1 3'UTR contains a potential miR-135b-binding site and exogenous miR-135b suppressed FOXO1 protein expression and its translational efficiency depending on the target site, clarifying

FOXO1 as a novel target of miR-135b (Figure 3D-F). Knockdown of miR-135b increased the protein expression of FOXO-dependent cell cycle inhibitors p21 and p27 as well as FOXO1 itself in ALCL cells (Figure 3G and supplemental Figure 2E). In Karpas 299 cells containing a barely detectable FOXO1, miR-135b suppression up-regulated p27 and alternatively another positive regulator of p27, CREG1 (supplemental Figure 2E).²⁰ Considering that NPM-ALK has been shown to inhibit FOXO3a activity through FOXO3a phosphorylation by AKT activation,²¹ NPM-ALK might thus regulate a wide range of FOXO family activities via protein modification and posttranscriptional regulation. Because FOXO factors are critical mediators in growth inhibitory responses to

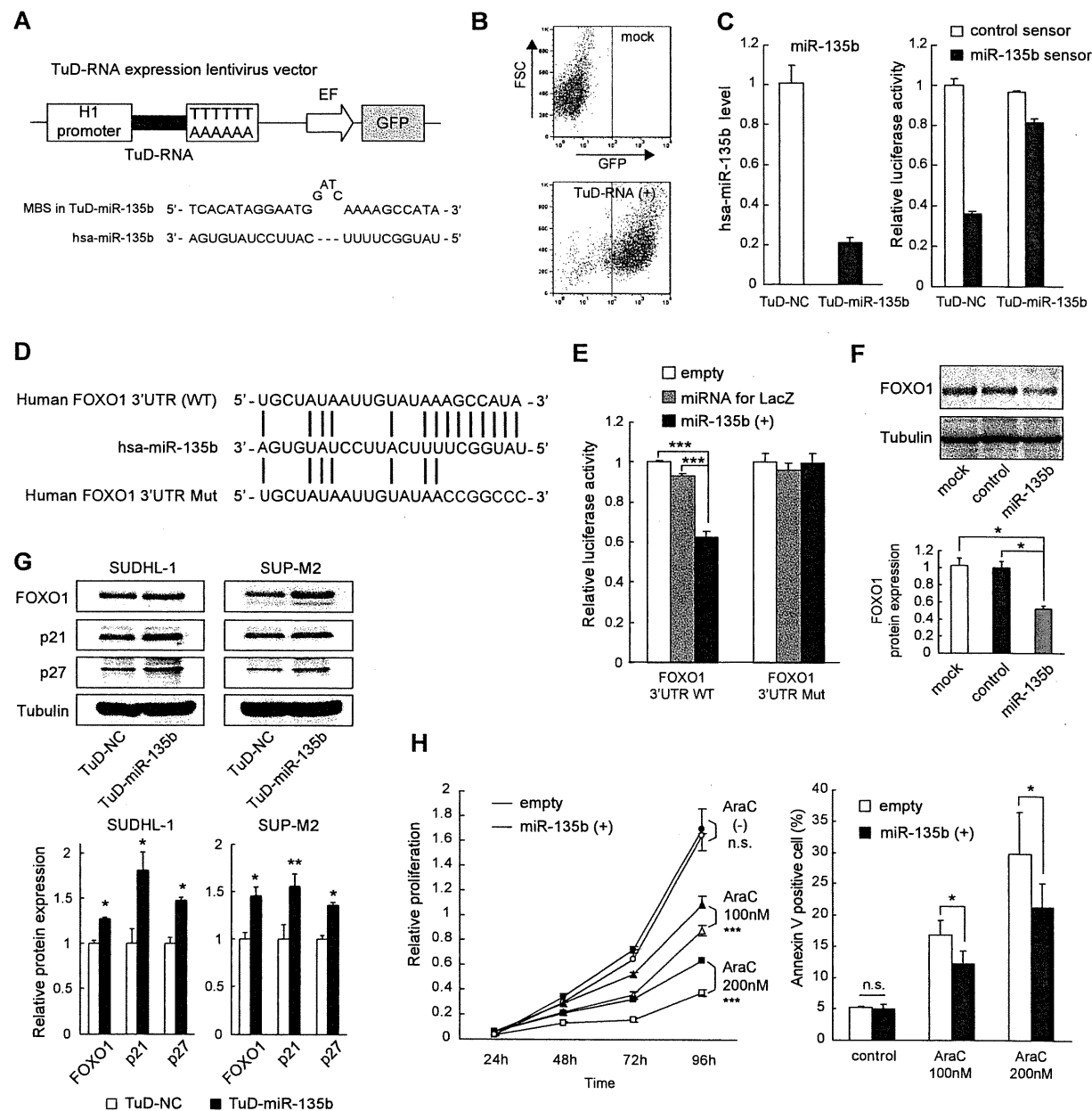


Figure 3. miR-135b targets FOXO1 and regulates chemosensitivity. (A) Structure of TuD RNA expression vector. TuD RNA for miR-135b contains miRNA-binding site (MBS) that is partially complementary to miR-135b. Details of TuD RNA structure have been described previously.¹¹ (B) Introduction of TuD RNA against miR-135b into ALCL cells. Flow cytometry profiles indicating transduction efficiency in Karpas 299 cells. FSC indicates forward scatter. (C) Inhibition of miR-135b function by TuD RNA for miR-135b. Left and right panels show qRT-PCR result and luciferase assay monitoring miR-135b activity, respectively. NC indicates negative control. (D) Sequence alignment between miR-135b and its putative binding site in the FOXO1 3'UTR. (E) miR-135b targets FOXO1. HEK293T cells were transfected with luciferase reporter containing the FOXO1 3'UTR with wild-type or mutated target site (shown in panel D), along with empty vector, miRNA-lacZ expression control vector (miRNA for lacZ), or pri-miR-135b expression vector [miR-135b (+)]. Luciferase assay was performed 48 hours after transfection ($***P < .001$). (F) Suppression of FOXO1 protein level by miR-135b. HeLa cells were transiently transfected with miR-135b and subjected to immunoblot analysis. (G) Elevated expression of FOXO1, p21, and p27 by miR-135b inhibition in ALCL cells. SUDHL-1 and SUP-M2 cells were infected with lentivirus harboring TuD-NC or TuD-miR-135b and applied to immunoblot analysis. The quantification results were shown in the bottom panel. (H) miR-135b-mediated attenuation of chemosensitivity. Jurkat cells with empty or pri-miR-135b vectors were treated with cytosine β -D-arabinofuranoside (AraC), followed by the assessment of cell viability (left) and apoptosis (right; $*P < .05$; $***P < .001$; n.s., not significant).

various stresses, including DNA damage,²² we examined the effect of miR-135b on the sensitivity to chemotherapeutic drugs to investigate functional consequences of FOXO1 alteration by miR-135b. Although miR-135 overexpression did not affect the proliferation of Jurkat cells under normal conditions, Jurkat cells overexpressing miR-135b were more resistant to cytosine β -D-arabinofuranoside (Figure 3H). These results suggest a possibility

that miR-135b may confer chemoresistance to ALCL cells through FOXO1 modulation.

Targeting of Th2 regulators STAT6 and GATA3 by miR-135b

It was shown previously that constitutive activation of ALK chimeric proteins is sufficient to induce cellular transformation and

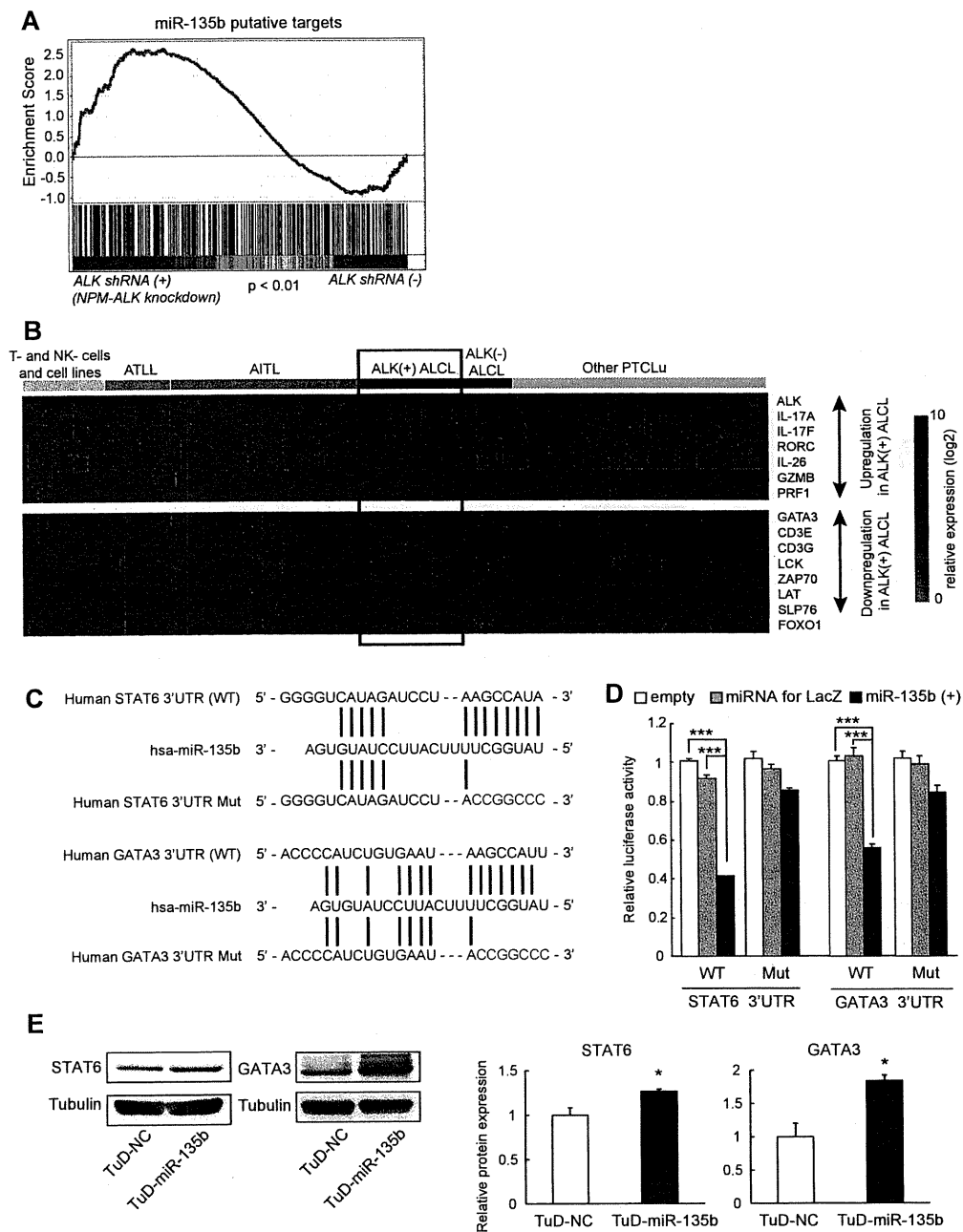


Figure 4. Targeting of STAT6 and GATA3 by miR-135b in ALCL. (A) Up-regulation of miR-135b target genes was evaluated on NPM-ALK knockdown using GSEA (dataset GSE6184). (B) Heat map showing the expression of Th17-related molecules, GATA3, FOXO1, and other ALCL-related genes (GZMB, PRF1, and TCR-related genes) in PTCL. Gene expression data are derived from GSE19069. In addition to GATA3, FOXO1 expression in ALCL was also lower than those in other PTCLs. ATLL indicates adult T-cell leukemia/lymphoma; AITL, angioimmunoblastic T-cell lymphoma; and PTCLu, PTCL-unclassifiable. (C) Sequence alignment between miR-135b and its putative binding sites in the STAT6 and GATA3 3'UTRs. (D) miR-135b targets STAT6 and GATA3. Luciferase activity of the STAT6 and GATA3 3'UTR reporter constructs with wild-type or mutated target site (shown in panel C) in HEK293T cells cotransfected with empty vector, miRNA-lacZ expression control vector (miRNA for lacZ), or pri-miR-135b expression vector [miR-135b (+)]; *** $P < .001$. (E) Up-regulation of STAT6 and GATA3 by TuD-RNA-mediated miR-135b inhibition in Karpas 299 cells. The quantification results were shown in the right panel.

that ALK activity is indispensable for the survival of ALK-positive ALCL cells.⁹ In the pathogenesis of ALCL, ALK elicits reproducible transcriptome changes, as shown by previous GEP analysis.¹² To gain insight for overall interconnection between NPM-ALK-driven gene response and miR-135b-mediated gene regulation, we performed GSEA using the GEP results of ALCL cells with or without shRNA-mediated NPM-ALK inhibition.^{12,16} GSEA demonstrated a significant up-regulation of miR-135b potential targets on NPM-ALK suppression, indicating that miR-135b constitutes an

arm of multiple NPM-ALK downstream pathways (Figure 4A and supplemental Figure 3A). This approach suggested TGFBR1, SIRT1, cyclin G2, CREG1, Bcl11b, and STAT6 as additional candidate targets of the NPM-ALK-miR-135b pathway.

ALCL of T-lymphocyte origin has been known to present with a T- or null-cell phenotype and lack TCR complex-related molecules such as CD3 ϵ and ZAP70, despite the presence of TCR rearrangements (Figure 4B).²³ Alternatively, recent GEP analysis in PTCL has demonstrated the following characters of ALCL cells: high

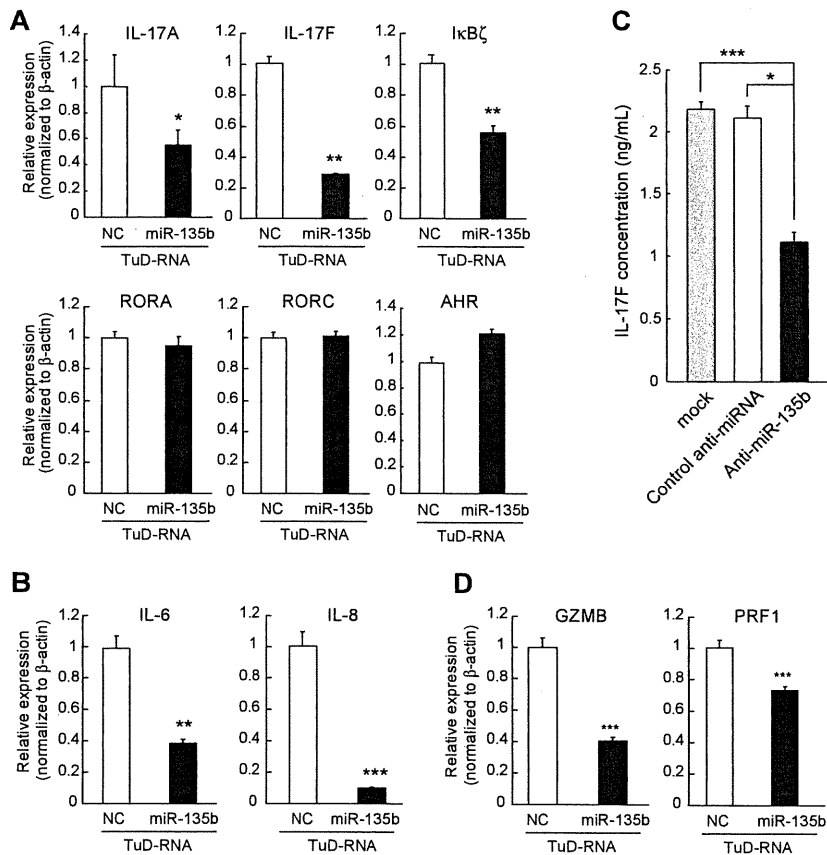


Figure 5. miR-135b blockade suppresses IL-17 production by ALCL cells and modulates ALCL immunophenotype. (A) Regulation of Th17-related molecules by miR-135b. Karpas 299 cells were infected with lentivirus harboring TuD-NC or TuD-miR-135b and applied to qRT-PCR analysis. Effects of miR-135b inhibition on the transcripts of Th17-related molecules were analyzed by qRT-PCR assay. Effects of miR-135b inhibition on IL-6 and IL-8 expression, as determined in panel A. (C) Effects of miR-135b inhibition on IL-17F production were analyzed in Karpas 299 cells by ELISA. (D) Effects of miR-135b inhibition on granzyme B (GZMB) and perforin 1 (PRF1) expression, as determined in panel A. miR-135b blockade did not affect the expression levels of IL-21, IL-23, and TGF- β 1 (data not shown; * P < .05; ** P < .01; *** P < .001).

expression of Th17-cell-associated molecules (IL-17A, IL-17F, and retinoic acid-related orphan receptor [ROR] γ), overlapping with Th17 cells phenotype, low expression of GATA3, and suppression of TCR components, as summarized in Figure 4B.¹⁵ Previous studies also have demonstrated that both Th1 and Th2 differentiation programs antagonize Th17-cell differentiation.²⁴

Along with these observations, reassessment of computational prediction proposed that miR-135b potentially targets 2 Th2 master regulators GATA3 and STAT6 (Figure 4C and supplemental Figure 3B). The GSEA result also supported the possibility of STAT6 as a miR-135b target (supplemental Figure 3A). We thus investigated the immune modulatory property of miR-135b on ALCL immunophenotype overlapping with Th17 cells. Luciferase assays revealed that miR-135b targets the 3'UTRs of both STAT6 and GATA3 (Figure 4D). Mutagenesis of potential target sites in their 3'UTR abrogated the response of STAT6 and GATA3 3'UTR to miR-135b, confirming direct interactions of miR-135b with STAT6 and GATA3 (Figure 4D). We further found that suppression of miR-135b indeed up-regulates protein expression of STAT6 and GATA3 in ALCL cells, demonstrating that both STAT6 and GATA3 are intrinsic targets of miR-135b in ALCL cells (Figure 4E and supplemental Figure 3C).

miR-135b blockade suppresses IL-17 production by ALCL cells

IL-4-STAT6 axis and GATA3 are important for Th2 differentiation of normal lymphocytes.²⁵ In normal lymphocyte differentiation, lineage-specific transcription factors can both activate and repress differentiation programs.^{26,27} GATA3 simultaneously promotes Th2 differentiation and represses Th1 differentiation, because Th1 regulator T-bet has opposing bidirectional effects.²⁵ A similar

relationship also exists between Th1 and Th2 differentiation programs and Th17 differentiation programs. As Th1 and Th2 effector cytokines (IFN- γ and IL-4) antagonize Th17 differentiation,²⁴ both GATA3 and T-bet have been shown to suppress Th17 differentiation.^{27,28} On the basis of these concepts, we next examined the effects of miR-135b suppression on the expressions of Th17-related molecules. Karpas 299 ALCL cells endogenously expressed IL-17, and miR-135b suppression attenuated the expression levels of IL-17A and IL-17F transcripts (Figure 5A), consistent with GATA3-mediated suppression of Th17 differentiation.²⁸ Blockade of miR-135b also suppressed the expression of I κ B ζ , a recently identified key regulator of Th17 differentiation,²⁹ without concomitant changes of ROR γ , ROR α , or aryl hydrocarbon receptor. In addition, down-regulation of proinflammatory cytokines including IL-6 and IL-8 was observed by miR-135b suppression (Figure 5B). Consistently, we confirmed that miR-135b suppression attenuates IL-17 production in Karpas 299 cells (Figure 5C). Taken together, these findings suggest that NPM-ALK/STAT3-miR-135b axis polarizes the identity of ALCL cells to the IL-17-producing immunophenotype resembling Th17 cells by suppression of GATA3 and STAT6. In addition, miR-135b knockdown suppressed the expression of granzyme B and perforin 1, cytotoxic molecules highly expressed in ALCL (Figure 5D),¹⁵ suggesting that miR-135b affects the broad range of ALCL immunophenotype.

Modulation of paracrine inflammatory reaction and tumorigenic potential of ALCL by miR-135b

IL-17 is a proinflammatory cytokine that stimulates the production of various inflammatory cytokines (eg, IL-1 β , IL-6, IL-8, G-CSF,

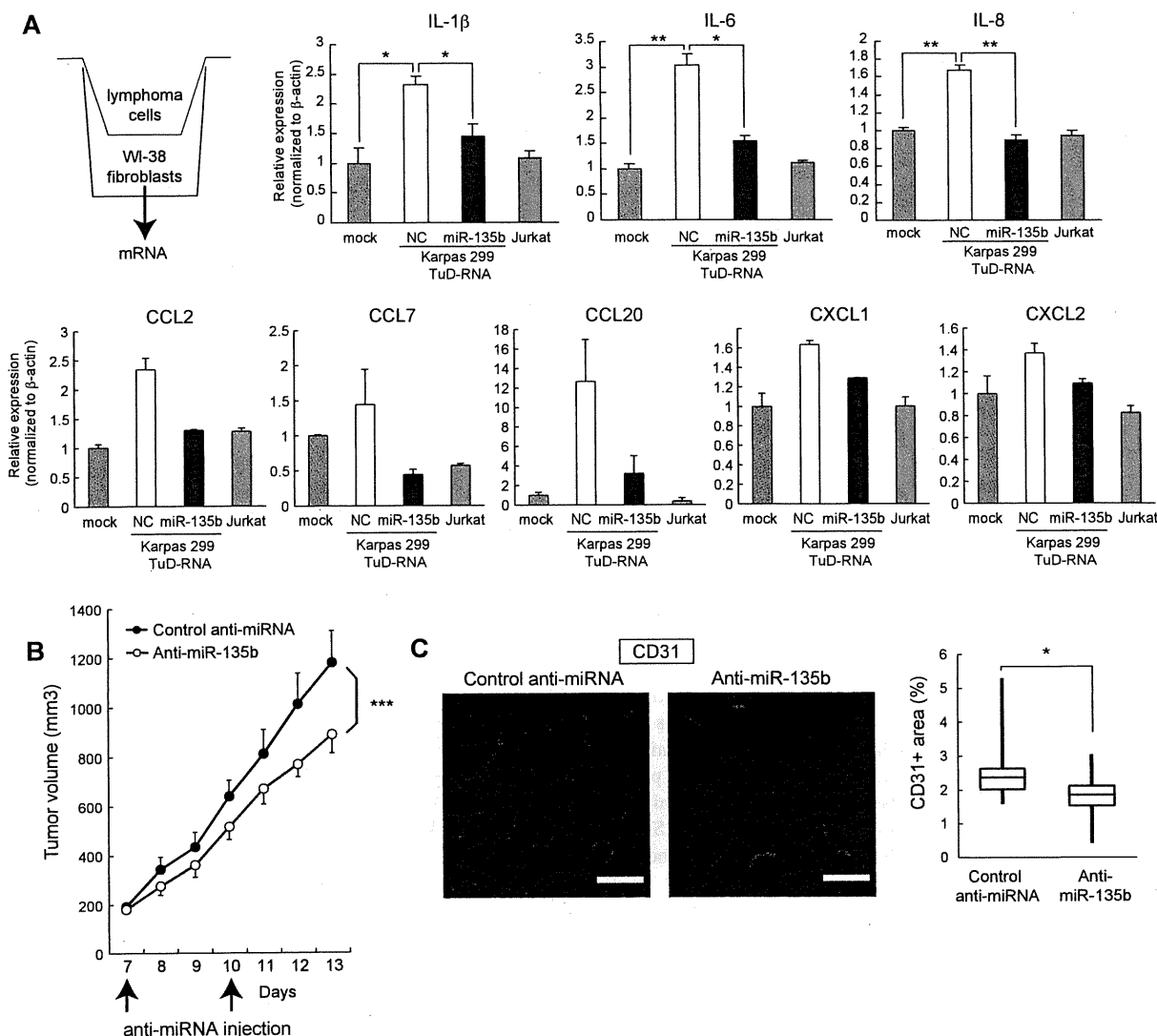


Figure 6. Regulation of paracrine inflammatory reaction and tumorigenic potential by miR-135b. (A) ALCL cells stimulate proinflammatory cytokine (IL-1 β , IL-6, and IL-8) and chemokine (CCL2, CCL7, CCL20, CXCL1, and CXCL2) production in human fibroblasts through an miR-135b-dependent manner. WI-38 human fibroblasts were cocultured with Karpas 299 or Jurkat cells and subjected to qRT-PCR assay (* $P < .05$; ** $P < .01$). (B) Growth curves of Karpas 299 subcutaneous tumors after transplantation into SCID mice and administration with miR-135 antisense-atelocollagen or control oligonucleotide-atelocollagen complexes. After random assignment at day 7 after inoculation ($n = 6$ /group), LNA-based antisense oligonucleotides (5 μ M) with atelocollagen were administered into the subcutaneous spaces around the tumors at days 7 and 10 and measured (means \pm SEM; *** $P < .001$). (C) Effects of miR-135b inhibition on tumor angiogenesis. Representative images of CD31 immunostaining of tumor sections (left) and quantification of microvessel density measured by CD31-positive area (right). Pixel density was quantified in multiple tumor images from 6 mice per group using ImageJ 1.36b software. Scale bar represents 100 μ m (* $P < .05$).

and GM-CSF) and chemokines (eg, CCL2, CCL7, CCL20, CXCL1, and CXCL2) from many cell types, such as fibroblasts, endothelial cells, and neutrophils, and is involved in pathogenesis of autoimmune disorders.³⁰ Although the significance of IL-17 in cancer is largely unknown and might depend on cancer-type and context, proinflammatory and proangiogenic properties of IL-17 have been associated with tumor progression in several studies.³¹⁻³⁴ In this setting, IL-17 has been shown to augment the secretion of angiogenic chemokines, such as CXCL1 and CXCL5.³⁴ We analyzed the operational role of miR-135b in tumor development of ALCL. Accordingly, coculture experiments demonstrated that Karpas 299 cells stimulate the production of proinflammatory cytokines (IL-1 β , IL-6, and IL-8) and chemokines (CCL2, CCL7, CCL20, and CXCL1/2) in WI-38 human

fibroblasts in an miR-135b-dependent manner (Figure 6A), underscoring the involvement of miR-135b in paracrine inflammatory response.

We also examined the roles of miR-135b in ALCL tumorigenic potential in vivo. In a xenograft model, local administration of LNA-based miRNA inhibitors against miR-135b with atelocollagen suppressed the growth of subcutaneous Karpas 299 tumors (Figure 6B). Furthermore, the inhibition of in vivo tumor growth by anti-miR-135b antisense was accompanied with reduced tumor angiogenesis (Figure 6C). These results thus collectively suggest that miR-135b-mediated modulation of paracrine inflammatory reaction favors tumor microenvironment, also indicating a therapeutic significance of targeting this axis by miR-135b interference.

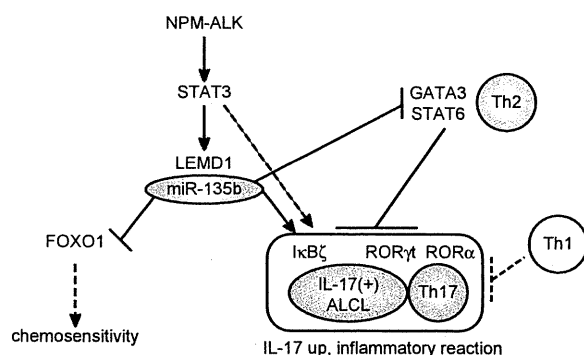


Figure 7. Summary of roles of miR-135b in ALCL pathogenesis. The present study demonstrates that NPM-ALK induces LEMD1 and miR-135b expression through STAT3 in ALCL and that miR-135b targets FOXO1 and two versatile Th2 regulators, GATA3, and STAT6, rendering the IL-17-producing immunophenotype to ALCL.

Discussion

Here, we identified miR-135b as a downstream mediator of NPM-ALK/STAT3 signaling (Figure 7). Although NPM-ALK drives malignant transformation of ALCL cells through various downstream signaling pathways, including STAT3, Ras-ERK, and PI3K,⁹ our study demonstrated the oncogenic aspect of miR-135b targeting FOXO1 in ALCL pathogenesis (Figure 7). It was shown previously that miR-135b is highly expressed in embryonic stem cells and other cancer types, including colorectal and prostate cancer.^{19,35,36} Considering the essential roles in embryonic stem cells and the pivotal oncogenic functions of STAT3,³⁷ the STAT3-miR-135b pathway might be widely used in these conditions. Oncogenic roles of miR-135b also might be supported by up-regulation of its host LEMD1, which is alternatively known as cancer/testis antigen 50, and DNA copy number gain in 1q32.1 in colorectal tumors.³⁸⁻⁴⁰ Although the biologic function(s) of LEMD1 has not been investigated so far, LEMD1 also might contribute to NPM-ALK-driven oncogenicity and IL-17-producing immunophenotype in ALCL. Considering other reports linking NPM-ALK to inhibition of FOXO3a activity through PI3K/Akt pathway,²¹ NPM-ALK might engage multiple players, including noncoding RNAs to prevent these central tumor suppressor pathways from activating by NPM-ALK-induced oncogenic stresses. We also examined miR-135b expression levels in lung cancer and neuroblastoma cell lines carrying ALK abnormalities (supplemental Table 4 and Figure 4). miR-135b expression was very low in neuroblastoma cell lines examined. The H2228 lung adenocarcinoma cell line containing EML4-ALK fusion expressed miR-135b to some extent, although at a lower level than ALCL cells. Involvement of miR-135b in the pathogenesis of some other tumor subtypes engaging ALK abnormalities remains to be further elucidated.

Importantly, we uncovered an interesting immune modulatory property of miR-135b. miR-135b targeted Th2 master regulators STAT6 and GATA3, and inhibition of miR-135b suppressed IL-17 production by ALCL cells, evidencing the Th17-skewing effect of miR-135b. ALK-positive ALCL is characterized by the presence of NPM-ALK and was originally described as a T- or null-cell phenotype. Loss of T-cell phenotype frequently observed in ALCL, shown by decreased expression of $\alpha\beta$ -TCR heterodimer and CD3 ϵ , has been demonstrated to be partly mediated by the perturbation by NPM-ALK signaling.²³ Conversely, it is postulated that the normal counterpart of ALCL is an activated mature cytotoxic T-cell,

because of the expression of cytotoxic granule-associated molecules such as TIA1, granzyme B, and perforin 1, although CD8 is usually negative in ALCL and CD4 is positive in 70% cases of ALCL.⁴¹ In addition to this aberrant phenotype, a recent molecular signature study of PTCL revealed that ALCL displays up-regulation of Th17-cell-associated molecules (IL-17A, IL-17F, and ROR γ) and down-regulation of GATA3. The immunophenotype overlaps with that of Th17 cells, compared with other lymphoma subtypes such as angioimmunoblastic T-cell lymphoma (AITL), ALK-negative ALCL, adult T-cell leukemia/lymphoma, and PTCL-unclassifiable.¹⁵ In support of this notion, a most recent report demonstrates that levels of IL-17, IL-8, and IL-22 were elevated in untreated ALK-positive ALCL patients' sera but undetectable in those of complete remission after chemotherapy,⁴² reinforcing the relevance of IL-17-producing immunophenotype of ALCL. Although the underlying mechanisms determining the immunophenotypes of various lymphomas have been largely unresolved, our study has demonstrated that a signaling network elicited by ectopic expression of NPM-ALK oncogene and its downstream miRNA confers the aberrant immunophenotype of ALCL cells.

Importance of tumor microenvironment in lymphoma development has been well investigated in B-cell lymphoma, including Hodgkin lymphoma.⁴³ A recent report has shown that IL-17-positive cells were more frequently observed in AITL than in PTCL-unclassifiable and that both Th17 and mast cells contribute to the lymphoma-associated proinflammatory environment in AITL.⁴⁴ In contrast, ALCL is unique in the respect that ALCL cells produce IL-17 by themselves, which might result in different clinical features between these lymphoma subtypes. In consistent with strong effects of IL-17 on neutrophils, extensive neutrophil infiltration has been observed in some cases of ALCL, as referred to as neutrophil-rich ALCL, which can sometimes be misdiagnosed as an inflammatory disease rather than lymphoma.⁴⁵⁻⁴⁷ Frequent B symptoms in ALCL also might be attributable to this IL-17-producing immunophenotype. In this study, antisense-based miR-135b blockade reduced tumor angiogenesis and growth in an in vivo tumor model, which observation is consistent with the proangiogenic function of IL-17 (Figure 6).^{33,34} Although a line of observations suggest both pro- and antitumor potentials of IL-17 or Th17 cells in a context-dependent manner,^{31,32} the tumor-suppressive effect of miR-135b inhibition suggests that local proinflammatory properties of IL-17-producing ALCL cells may provide the favorable tumor microenvironment through the enhancement of angiogenesis or so in this context. Recent evidence has revealed that many characteristic aspects of cancer-related biologic processes, including drug resistance, maintenance of cancer-initiating cells, and metastasis, are associated with miRNA function.⁴⁸ The present study demonstrates another unique contribution of miRNA dysregulation to tumor development, ie, modulation of immunophenotype of lymphoma cells and the consequent alteration of tumor milieu by miR-135b.

Among hundreds of miRNAs, miR-326 has been identified so far as a regulator of Th17 differentiation, which promoted Th17 differentiation via targeting ETS1.⁴⁹ In addition, miR-155 was recently shown to promote Th17 cell formation in a CD4⁺ T-cell intrinsic manner.⁵⁰ It was consistent with the finding that miR-155 targets Th2 promoter c-Maf. Our study suggests the presence of additional regulatory miRNAs of Th17 differentiation through the inhibition of differentiation program(s) to other helper T-cell lineage(s). Generally, lineage-specific transcription factors and cytokines can interfere with the differentiation to other helper T-cell subsets. Although it requires careful assessment about